NAVAL POSTGRADUATE SCHOOL
MONTEREY, CALIFORNIA

THESIS

DETECTION OF OCEANIC CONVECTION
UTILIZING
SUBMARINE-OBSERVED ACCELERATION

by

Kevin F. Bedell

June, 1995

Thesis Advisor: Roland W. Garwood, Jr.
Co-Advisor Arlene A. Guest

Approved for public release; distribution is unlimited.

REPORT DOCUMENTATION PAGE

Form Approved OMB No. 0704-0188

1. AGENCY USE ONLY *(Leave blank)*	2. REPORT DATE June, 1995	3. REPORT TYPE AND DATES COVERED Master's Thesis

4. TITLE AND SUBTITLE DETECTION OF OCEANIC CONVECTION UITLIZING SUBMARINE-OBSERVED ACCELERATION

5. FUNDING NUMBERS

6. AUTHOR(S) Bedell, Kevin F.

7. PERFORMING ORGANIZATION NAME(S) AND ADDRESS(ES)
Naval Postgraduate School
Monterey CA 93943-5000

8. PERFORMING ORGANIZATION REPORT NUMBER

9. SPONSORING/MONITORING AGENCY NAME(S) AND ADDRESS(ES)

10. SPONSORING/MONITORING AGENCY REPORT NUMBER

11. SUPPLEMENTARY NOTES The views expressed in this thesis are those of the author and do not reflect the official policy or position of the Department of Defense or the U.S. Government.

12a. DISTRIBUTION/AVAILABILITY STATEMENT
Approved for public release; distribution is unlimited.

12b. DISTRIBUTION CODE

13. ABSTRACT *(maximum 200 words)*

The feasibility of using submarine-recorded acceleration and navigational data to detect deep convection in the ocean was explored by comparing actual submarine observations of vertical velocity with vertical velocity of a hypothetical submarine driven through a field of oceanic turbulence predicted by Large-Eddy Simulation (LES). The actual submarine data included time series of three-dimensional acceleration and submarine velocity from the inertial navigation system (INS), gravity and keel depth. Of all these fields, vertical velocity derived from the INS proved most useful for comparison with the simulated vertical velocity fields. The actual observations were analyzed as a function of submarine depth and speed. The spectral energy density was computed for several standard depths, with the largest vertical accelerations found for the times when the submarine was at the shallowest depths. Spectral shape also varied with depth, with the strongest high-frequency /wavenumber intensity for the shoalest cases. The submarine may have experienced a combination of surface gravity wave motion and mixed layer turbulence in the shallowest case, but there was probably no significant oceanic convection at any of the other depths because of stability of the water column. Spectra of the hypothetical submarine transiting an LES-predicted field of turbulence were contrasted with the spectra of the observed vertical velocity. Although the observed signal's spectral intensity exceeded the spectral intensity for the highest frequency motions of the simulated turbulence, the LES predicted convection intensity for scales greater than 400m was significantly greater than the corresponding signal obtained for the submarine during times when the submarine was not encountering oceanic turbulence. Hence, the background accelerations attributable to vessel propulsion and hydrodynamics or to surface effects during normal operations should not mask the accelerations it would experience if it transited significant deep oceanic convection. It was concluded that such a submarine could be an excellent tool for observing and monitoring the most significant deep oceanic convection.

14. SUBJECT TERMS submarine observations, gravity measurements, convection, turbulence, Large Eddy Simulation

15. NUMBER OF PAGES 95

16. PRICE CODE

17. SECURITY CLASSIFICATION OF REPORT Unclassified	18. SECURITY CLASSIFICATION OF THIS PAGE Unclassified	19. SECURITY CLASSIFICATION OF ABSTRACT Unclassified	20. LIMITATION OF ABSTRACT UL

NSN 7540-01-280-5500

Standard Form 298 (Rev. 2-89)
Prescribed by ANSI Std. 239-18 298-102

Approved for public release; distribution is unlimited.

DETECTION OF OCEANIC CONVECTION UTILIZING SUBMARINE-OBSERVED ACCELERATION

Kevin F. Bedell
Lieutenant Commander, United States Navy
B.S., United States Naval Academy, 1983

Submitted in partial fulfillment
of the requirements for the degree of

MASTER OF SCIENCE IN PHYSICAL OCEANOGRAPHY AND METEOROLOGY

from the

NAVAL POSTGRADUATE SCHOOL
June 1995

Author: Kevin F. Bedell
Kevin F. Bedell

Approved by:
Roland W. Garwood, Jr., Thesis Advisor

Arlene A. Guest
Arlene A. Guest, Co-Advisor

Robert H. Bourke
Robert H. Bourke, Chairman, Department of Oceanography

ABSTRACT

The feasibility of using submarine-recorded acceleration and navigational data to detect deep convection in the ocean was explored by comparing actual submarine observations of vertical velocity with vertical velocity of a hypothetical submarine driven through a field of oceanic turbulence predicted by Large-Eddy Simulation (LES). The actual submarine data included time series of three-dimensional acceleration and submarine velocity from the inertial navigation system (INS), gravity and keel depth. Of all these fields, vertical velocity derived from the INS proved most useful for comparison with the simulated vertical velocity fields. The actual observations were analyzed as a function of submarine depth and speed. The spectral energy density was computed for several standard depths, with the largest vertical accelerations found for the times when the submarine was at the shallowest depths. Spectral shape also varied with depth, with the strongest high-frequency/wavenumber intensity for the shoalest cases. The submarine may have experienced a combination of surface gravity wave motion and mixed-layer turbulence in the shallowest case, but there was probably no significant oceanic convection at any of the other depths because of stability of the water column. Spectra of the hypothetical submarine transiting an LES-predicted field of turbulence were contrasted with the spectra of the observed vertical velocity. Although the observed signal's spectral intensity exceeded the spectral intensity for the highest frequency

motions of the simulated turbulence, the LES-predicted convection intensity for scales greater than 400m was significantly greater than the corresponding signal obtained for the submarine during times when the submarine was not encountering oceanic turbulence. Hence, the background accelerations attributable to vessel propulsion and hydrodynamics or to surface effects during normal operations should not mask the accelerations it would experience if it transited significant deep oceanic convection. It was concluded that such a submarine could be an excellent tool for observing and monitoring the most significant deep oceanic convection.

TABLE OF CONTENTS

ACKNOWLEDGEMENTS

I would like to thank my advisors, Professor Roland W. Garwood and Ms. Arlene A. Guest for their support, guidance, and patience in the research and preparation of this thesis. I would also like to thank Mr. Ramsey Harcourt for his support. I would like to thank Dr. Bernie Epstein from Strategic Systems Programs for providing the submarine GSS data which made this research possible. Additionally, I would like to thank the Arctic Submarine Laboratory for their aid and support. Finally, I would like to thank my fiancee Gail, for her patience and support throughout the preparation of this thesis.

I. INTRODUCTION

Turbulence in the ocean is difficult to observe and quantitatively measure because it is a complex function of space and time, and because there are a variety of mechanisms for its generation, transformation and dissipation. Field experiments in the Mediterranean and the Greenland Sea have measured turbulence with a Eulerian approach and have experienced limited success primarily due to measuring device limitations. Valuable computational and observational tools such as the Large Eddy Simulation (LES) model and an operational submarine when used together have the potential to greatly improve our understanding of turbulent convection in the ocean. The submarine can survey vast areas with relative ease while remaining beneath hazardous surface conditions.

By utilizing onboard instrumentation designed to measure and record the vertical acceleration that the submarine experiences, a subsurface platform can quantitatively map a broad area of the polar or sub-polar seas and provide vertical convection data. These data could then be processed to extract a signal for positive identification of turbulence and comparison with the known turbulence signal generated by the LES. This information, collected with minimal impact on a submarine's normal operating routine, will be valuable for gaining knowledge on the deep

convective mixing mechanisms that initiate the global thermohaline circulation and the meridional transport of heat, which in turn strongly influences the world's climate. To date, submarine voyages collecting CTD, and passive and active acoustic data have been instrumental in delineating the layered nature of the Arctic Ocean (McClaren, 1985). Also, through the measured variability of the speed of sound due to changing temperature, pressure and salinity, accurate measurements of the magnitude and direction of currents, internal waves, tides and large scale fronts and eddies are feasible (McClaren, 1985). The submarine conducts operations in the mixed layer which could potentially be adversely influenced by strong turbulence. Effective use of the submarine could be invaluable to better understand the convection process and to more accurately model it in strategically significant regions such as the Arctic and Mediterranean Seas. The submarine, uniquely equipped for polar sea exploration, has great potential as an asset for scientific research that would benefit applied science and technology and facilitate safer, more efficient USN operations.

The convective environment chapter will provide a general background of the Arctic region with emphasis on convection generating processes, buoyancy and the thermal heat balance and how they interact to inhibit or augment turbulence. A brief review of two experiments conducted in the polar seas will point

out two approaches that had some success detecting turbulence. Gravity theory will be presented with emphasis on how it has been measured and the considerations necessary for analysis.

In this study the feasibility of utilizing submarine-recorded acceleration and gravity from onboard instrumentation to detect turbulence will be explored. The LES model will be utilized to produce a simulated field of turbulence that could represent what a submarine might experience if transiting an area of active turbulent convection. Figure 1, produced by the LES model, depicts horizontal velocity and temperature changes on a horizontal plane in the oceanic turbulent boundary layer. Figure 2, also produced by the LES model, displays the vertical velocity for the same region as Figure 1. The red represents downward motion and the blue is upward motion caused by the horizontal convergence depicted in Figure 1. A simulated submarine will be driven through these model-generated fields utilizing the "frozen eddy" hypothesis which enables spatial derivatives to be converted to time derivatives, including acceleration, dw/dt. Hence, simulated dw/dt in the LES may be compared to actual observations of acceleration aboard a submarine.

The submarine records keel depth, vertical velocity and vertical acceleration with three different onboard sensors. The submarine-recorded data was partitioned according to four depths: standard depth 1 (SD1), standard depth 2 (SD2), standard

depth 3 (SD3) and standard depth 4 (SD4). SD1 is the shallowest and is assumed to be within the mixed layer, while the other levels increase in depth below the mixed layer with SD4 the deepest. Data from the three different sensors for the standard depths will be analyzed to determine which instrument yields the most useful information from which to potentially detect turbulence. The LES-produced fields of vertical velocity and acceleration will be contrasted with the submarine fields. The final chapter will summarize significant findings and provide recommendations for future submarine detection of convection.

II. THE CONVECTIVE ENVIRONMENT

Although turbulence is nearly ubiquitous in the surface boundary layers of all bodies of water because of the nearly perpetual momentum and heat exchange with the atmosphere, there are certain locations where it may be especially important and yet difficult to observe. The Arctic Ocean and the surrounding Polar Seas is a harsh environment which experiences extreme cooling and ice formation. This intense thermal energy exchange between the atmosphere and the water coupled with strong winds drives strong convection that creates deep mixed layers and may be connected to the deepest oceanic mixing. A background understanding of the processes that generate and influence convection is valuable for this study and the Arctic regime is a prime location for this purpose.

A. SURFACE HEAT BALANCE

The Arctic Ocean influences global exchanges and climate. This influence is manifested through the local radiation balance by disposing of excess heat produced in the tropics and sub-tropics. Another influence is through thermohaline circulation.

Figure 3a, from Aagaard and Carmack (1994), is a schematic depicting processes that modulate various fluxes in the Arctic basin. Heat fluxes in the Arctic Ocean occur primarily along the periphery where leads, polynyas and seasonal open water areas

allow the heat exchange to take place. The interior of the Arctic Ocean experiences a considerably smaller annual net surface heat flux due to stratification from 50-150m (Aagaard and Carmack, 1994). Because of this, vertical diffusion rates are reduced and the surface waters of the upper water column are insulated from the warmer Atlantic layer below. This stratification restricts convective and surface layer mixing to depths generally less than 50m (Aagaard and Carmack, 1994). This buffering of the heat in the Atlantic layer by the stratification is the principal reason why the Arctic Ocean maintains a year-round ice cover.

Aagaard and Carmack (1994) suggest that anomalously warm inflow from the Bering Strait and/or flow from the continental shelves results in near surface temperatures being above the freezing point even during the winter. Changes in vertical structure could be initiated from this positive temperature anomaly which could have significant impact on convective and diffusive fluxes of salt and sensible heat across the pycnocline and the mixed-layer interface. Ice model sensitivity studies (e.g., Maykut and Untersteiner, 1971) indicate that an increase in the vertical heat flux may reduce ice cover that could change the surface and atmospheric radiation heat balances. The most significant factor is that strong stratification has a direct

impact on the ice cover and consequently upon air-sea fluxes of heat and momentum.

B. CONVECTIVE OVERTURNING

Surface-driven convection is dependent upon ice conditions and prevailing stratification. Winter cooling alone is unable to drive convection to the bottom of the deep basins of the polar seas due to the strongly stable conditions created by low salinity surface water overlying significantly more saline water. Figure 3b depicts the circulation and water mass structure in the Arctic Ocean. Ice formation is reduced when intense surface cooling produces denser saline water which sinks and destablizes the water column. This causes heat diffusion that reduces the surface ice cover. The Greenland Sea is known to be a major deep-water formation area, with the largest density gradient found close to the sea surface (Aagaard et al., 1985). It appears that convection in the Greenland and Iceland Seas is conditioned by freshwater export from the Arctic Ocean (Aagaard and Carmack, 1989). It is hypothesized that at some level of increased export, convection would cease due to increased buoyancy. Northward transport of Atlantic water would decrease, and the ice cover would spread southward. Conversely, if the supply of freshwater to the Arctic were to decrease, the stratification in the Eurasian basin might weaken. Increased convection would result

that would enable more effective northward heat transport and a consequent decrease in ice cover.

Open-ocean convection in the Greenland Sea and near-boundary convection around the perimeter of the Arctic Ocean represent the two major sources of deepwater formation. As depicted in Figure 3b, open-ocean convection in the Greenland gyre may reach the bottom, while in the Iceland Sea, convection reaches only to mid-depth. The isopycnals in Figure 3b separate surface, intermediate and deep waters. There is evidence that there is shelf water of sufficient density in the winter to displace deep water, but no actual observations of convection along the continental slope exist (Aagaard et al., 1985). Although the production of deep and intermediate waters necessary to drive circulations such as those depicted in Figure 3b are not well understood, a recent theory proposes a preconditioning phase which slowly removes the initial stratification followed by a deep mixing phase where local heat fluxes deepen the mixed layer to 1500m or more (Pawlowicz et al., 1995).

During the deep mixing phase, vertical velocities can reach 2-10cm/s, and as this water sinks, it also spreads horizontally. Deep convective plumes are capable of transporting and mixing water over hundreds of meters in a time frame of hours to days (Aagaard and Carmack, 1989). As deep convection takes place, across-isopycnal advection produces

intermediate and bottom water and strongly influences the vertical structure of deep water masses. These water masses eventually influence the deep circulation patterns which have an effect on the meridional heat transport within the ocean (Paluskiewicz et al., 1994).

The equation of state for the density of sea water is highly nonlinear for cold water near freezing. Of particular importance is the thermobaric effect, in which the thermal expansion is highly dependent upon depth or pressure. The thermobaric effect can result in two types of conditional instabilities. A parcel instability or a layer instability each have the capability to release seasonally stored potential energy. For either of these instabilities to occur a water parcel or water column that was hydrostatically stable at the surface must sink and become hydrostatically unstable with depth (Garwood et al., 1994). A parcel instability occurs when a parcel in the mixed layer penetrates below a critical depth and attains a density greater than that of the surrounding water. The parcel may then continue to sink through the mixed layer and penetrate the pycnocline (Garwood et al., 1994). In a layer instability, downwelling initiated by large-scale convergence or by preconditioning associated with larger scale dynamics forces the whole layer to subside. This mechanism may be responsible for convective plumes even when there is no surface forcing (Garwood et al., 1994).

C. HALOCLINE

In the Arctic Ocean, the halocline is a layer of cold water three to four times as thick as the upper low-salinity layer (Figure 4a). At cold temperatures, density becomes much more salinity-dependent; thus, the halocline is coincident with the pycnocline. The halocline acts as an insulating barrier and inhibits the upward heat flux from the warm Atlantic layer preventing it from mixing with the colder upper layer and thus reducing the potential sensible heat influence on the ice cover and atmosphere. The isohaline layer establishes the depth limitation of convective mixing created by salt separation during freezing (Aagaard et al., 1981). If the convection is strong enough, it can deepen the halocline. It was previously believed that the halocline was maintained by a mixture of surface and Atlantic waters but this mixture could not account for the cold temperatures measured in the upper halocline. Salinity values as high as those discovered in the upper halocline are never found very close to the surface in the central Arctic, and a mixed layer source is unlikely (Coachman and Barnes, 1962). Figure 4b depicts a possible mechanism for halocline maintenance where cold (near the freezing point) saline (34 psu or more) water is advected from peripheral sources such as the continental slope and submarine canyons. The distribution of nutrients in the upper halocline is further evidence that advection may be taking place (Aagaard et al., 1981).

III. OBSERVATIONS OF CONVECTION

Observations of convection are very limited and few experiments have yielded positive results. Experiments by Schott et al., (1993) and Scott and Killworth (1991) are presented as examples that have significantly improved our understanding of deep oceanic convection in the Polar Seas.

A. ADCP OBSERVATIONS

During the winter of 1988-1989 five acoustic doppler current profilers (ADCP) were moored in the central Greenland Sea to measure currents that may be associated with deep mixing and convection (Schott et al., 1993). Two ADCP's scanned upward from about 300m with attached thermistor strings, which recorded temperature stratification from 60-260m. Two ADCP's scanned downward from 200m and one scanned upward from 1400m. The mean wind conditions were northerly due to high pressure over Greenland and lower pressure over the Atlantic Ocean. The European Center for Medium-Range Weather Forecasts (ECMWF) model provided wind stress fields and heat flux components at six-hour time intervals. During the fall to winter of 1988 the ice expanded eastward from the east coast of Greenland. By late December the ice-covered region reached its farthest extent (Figure 5). In mid-January an area of ice-free water began to form creating a long wedge of ice curled around the central Greenland Sea called "is odden," and the ice-free area

enclosed by it called "nordbukta". The central Greenland Sea is an area of significant doming, both isopycnal and isothermal. The 0C isotherm rises from below 500m depth to above 50m over a distance often less than 100km. Due to doming, the surface mixed layer depth in the center of this region is at a minimum and it is here that stability can most readily be overcome by the surface cooling, evaporation or brine rejection (Schott et al., 1993). At mooring position 319, with the onset of ice coverage, cooling to near-freezing temperatures thickened the mixed layer from 60m in late November to 200m in late January. Over this time period, salinity within the mixed layer increased, thus reducing stability and preconditioning the water column for deep mixing.

Figure 6a depicts a time series of unfiltered vertical velocity data from September 1988 to April 1989 from 160m depth at station 319. A mean bias was present which was always negative due to internal ADCP data processing. There was a diurnal cycle (mean amplitude of 1 cm/s), particularly noticeable below the surface mixed layer in September-October and in February-March due to vertical migration of zooplankton scatterers. The velocity variations of interest were short period fluctuations with amplitudes larger than the diurnal cycle which occurred November 17-23 and February 14-16. High-frequency variance of the vertical velocity (W'^2) in homogeneous water is a good indicator of convective activity.

Figure 6b depicts the band passed (periods >6 and <2 hours eliminated) variance of vertical velocity for several depths of each of the five ADCP's. The first W'^2 event at station 319 occurred in early October simultaneously with the first cooling event of the season. November's pronounced peak occurred in conjunction with a burst of northerly winds and second strong cooling event of the season. These fluctuations were determined to be internal waves generated by convective activity in the shallow mixed layer where cooled fluid parcels impinged on the stratified water below. In late January, southward wind bursts with heat losses of $>500 w/m^2$ were coincident with significant vertical velocity variance maxima. Mixed layer deepening was observed during this period but a correlation with particular downward velocity events could not be established. February cooling which deepened the mixed layer to below 347m, created a large region of homogeneous water which was preconditioned for deep convection subsequently observed in early to mid March. On March 16 a sharp temperature drop was recorded at station T6 in 1400m depth of water (Figure 7a). Downward motion recorded by ADCP's was 3-5cm/s in both the 1100-1400m and 200-500m depth range (Figure 7b). Overall the W'^2 values of the Greenland Sea in the winter of 1988-1989 were small ($<2 cm^2/s^2$) below the near-surface layer.

B. TOWED THERMISTOR OBSERVATIONS

Scott and Killworth (1991) analyzed experimental measurements from a thermistor chain tow north of Iceland in August 1987, near 69°N, 18°W. Supplementary data included seven closely spaced CTD profiles from the same region taken 14 days prior to the chain tow. The chain was towed by the MV SEA SEARCHER transiting at 4 knots in calm weather. Figure 8 shows two vertical cold structures about 3km wide. These structures are distinguishable below the characteristic cold sub-layer of the region, beginning at approximately 70m. Scott and Killworth call the features "chimneys" which in this case contain water that is 1.2C cooler than surrounding water, and extend to the maximum depth of the chain data (270-280m). This situation is atypical in that the atmospheric boundary layer plays no role in the exchange of water between layers. In this case the surface layer at about +7.5C is de-coupled from the chimneys by the cold sublayer, which attains a minimum of about -1.5C at around 30-40m depth. No influence of the chimneys is detectable in the warm surface layer. It is not clear how these features were produced. The surface is capped by the warm surface layer, thus reducing the possibility of air-sea interaction as a forcing mechanism. Scott and Killworth speculated that the lateral density contrast between a chimney and its environment was around $0.01 kg/m^2$, although the change in ambient stratification through which the chimney sank was significantly

greater than this value. Thus, the water in the chimney could only sink a fraction of the vertical distance observed before becoming neutrally stable. The dilemma is that the chimneys do not appear to be dense enough to sink to observed depths, and the surrounding water is too stably stratified. Other possibilities explored by Scott and Killworth included double diffusion and lateral double diffusion but both these theories lacked supporting evidence.

Although many questions remain on how these chimneys are produced, the chimneys form an important link between the surface and the deep ocean. Schott et al's. experiment involved a Eulerian approach utilizing moored instruments, while Scott and Killworth utilized a Lagrangian approach with towed instruments. Both are valuable data sets of observed convection but represent expensive and difficult means to acquire data that can be adversely impacted by poor weather. Hazardous surface conditions will not impede a submarine from collecting data; in fact, it would increase the likelihood of encountering turbulence.

IV. THEORY AND SIMULATION

A. GRAVITY

One component of acceleration acting on a submarine is gravity. Observations of apparent gravity by a submarine will include vertical accelerations that may be attributable to oceanic turbulence. For this reason, gravity observations are of interest here. Gravitational force is an attracting force which exerts an influence between the earth and every object that is located within, on or above the earth's surface. All objects within or on the earth's surface follow a circular path due to the earth's rotation, and in doing so exert an outward force, the centrifugal reaction. The sum of the gravitational force and centrifugal reaction acting upon an object is called gravity. The gravitational force is significantly greater than the centrifugal reaction and thus causes an object to have weight. If the object is free to fall, the acceleration experienced by that object as it moves toward the center of the earth is called the acceleration of gravity, which is the quantity observed when gravity measurements are made. G force is a term used in aviation associated with acceleration due to gravity in an aircraft. A G factor of one indicates the acceleration due to the attraction of the earth and is considered a neutral condition. A G factor of one is approximately equal to one thousand gals, a unit named after

Galileo. The milligal (mg), one-thousandth of a gal, is commonly used for the small variations in acceleration measured in this type of study. One gal is equal to one centimeter per second squared.

Two different types of gravity measurements can be recorded: absolute gravity and relative gravity. If the value of acceleration of gravity can be determined at the point of measurement directly from the data observed at that point, the gravity measurement is absolute. If only the differences in the acceleration of gravity are measured between two or more points, the gravity measurement is relative.

1. Gravity Measurement

Gravity measurement onboard a submarine is an involved process which attempts to attenuate the effects of random submarine vertical motion to ultimately record the earth's gravity for navigational purposes. The measurement is complicated by several disturbing forces which produce a significant error contribution. Mays and Falchetti (1978) performed a gravity measurement analysis where they developed an equation to relate the gravity measurements to presurveyed map reference values. The Naval Air Development Center Gravity Range was used to generate reference values for comparison with measured gravity values. Their analysis is presented as an example of one method of processing gravity and the many considerations that are inherent in its calculation.

Gravity measurements collected by a submarine include actual gravity plus effects of disturbing forces, including ocean turbulence. To minimize the effect of these forces on the gravity measurements, compensation equations have been developed. A representative statistical model of the gravity anomaly field used in conjunction with compensation equations were used by Mays and Falchetti (1978) to estimate residual error terms. The objective of gravity processing is to apply compensation/ filtering techniques to minimize the errors that the terms in (1), which relates the gravity measurements to the presurveyed map reference values, may introduce.

$$
\begin{aligned}
a(t) = G_{map}(X_{ref}, Y_{ref}, 0) - \frac{\partial}{\partial X} G_{map} | \delta X_{(X_{ref}, Y_{ref}, 0)} \qquad (1) \\
- \frac{\partial}{\partial Y} G_{map} | \delta Y_{(X_{ref}, Y_{ref}, 0)} - E_{map}(X_{ref}, Y_{ref}, 0) \\
- \frac{\ddot{\ }}{Z_{ref}} + \frac{\ddot{\ }}{\delta Z} + E_{I} + E_{tides} - E_{down}(X_{ref}, Y_{ref}, Z_{ref}) \\
- G_{down}(X_{ref}, Y_{ref}, Z_{ref}) + \frac{\partial}{\partial Z} G_{down} | \delta Z_{(X_{ref}, Y_{ref}, Z_{ref})}
\end{aligned}
$$

The inertial accelerometer mounted onboard a moving submarine senses a force "a". The instrument's sensitive axis is aligned to the local vertical axis. The force "a" is the sum of the true gravity field G_{true}, the kinematic vertical acceleration vector Z_{true}, tidal accelerations E_{tides}, and instrumentation noise E_{I}. This yields:

$$a(t)=G_{true}(X_{true}, Y_{true}, Z_{true})-\ddot{Z}_{true}+E_{I}+E_{tides}$$

where (X_{true}, Y_{true}, Z_{true}) is the true acceleration position vector and time dependencies are implicit.

Mays and Falchetti expressed the force "a" in terms of the value of gravity given by the applicable reference surface map. G_{map}, the reference surface map value, is a function of the horizontal coordinates only and differs from the true field due to survey errors $E_{map}(X_{true}, Y_{true}, 0)$ and downward continuation corrections which relate measurements at depth to measurements on the surface. Due to the inability to accurately determine the downward continuation correction G_{down}, a residual error term E_{down} is included. This yields:

$$G_{map}(X_{true}, Y_{true}, 0)=G_{true}(X_{true}, Y_{true}, Z_{true})+G_{down}(X_{true}, Y_{true}, Z_{true})+E_{down}(X_{true}, Y_{true}, Z_{true})+E_{map}(X_{true}, Y_{true}, 0)$$

Although the true position vector and vertical accelerations are never actually determined, they are related to the reference position by:

$$\begin{aligned} X_{ref}&=X_{true}+\delta X \\ Y_{ref}&=Y_{true}+\delta Y \\ Z_{ref}&=Z_{true}+\delta Z \\ \ddot{Z}_{ref}&=\ddot{Z}_{true}+\overline{\delta Z} \end{aligned}$$

Navigation errors, depth gauge errors and lever arm effects between the navigation sensor units and the gravity sensor contribute to the disparity between true position vector and reference position. Position error dependencies in E_{map} and E_{down} are considered second order effects and can be neglected. Sensor motion effects can be grouped into one category known as Eotvos effects and translational vertical acceleration effects due to direct displacement of the submarine as measured by the Submarine Inertial Navigation System along the local vertical axis. Eotvos is characterized by bias which could not be eliminated with filtering techniques; thus a measurement compensation technique was introduced which will not be discussed here.

Equation (1) defines the terms which relate the presurveyed map reference values to the gravity measurements. Measurement terms whose spectral content exceed the spectrum of the local gravity field can, through filtering, have their effects attenuated with no loss of useful gravity data. Measurement terms whose spectral content overlaps the gravity field spectrum cannot be filtered without inducing distortion to the gravity field measurements. To correct this, deterministic compensation procedures must be employed or their effects must be tolerated.

2. Gravity Measuring System

The equipment used to measure and record gravity data in the Mays and Falchetti analysis was the BGM-3 Gravity Measuring System designed by Bell Aerospace Division, Textron Corporation for shipboard operations. The gravity measuring accelerometers onboard the submarine which recorded the observed gravity data for this study function similar to the BGM-3. Two functional groups make up the gravity measuring system; the gravimetric sensor group and the data acquisition group.

The gravimetric sensor group consists of a sensor and sensor electronics unit, stabilized platform and platform electronics unit. It measures forces along the local vertical axis and converts the measurements into a digital format to facilitate compatibility with the data acquisition group. The primary component of this sensor group is the Bell Model XI accelerometer mounted in a vertical configuration on the system stabilized platform. Gravity and other accelerations all influence the accelerometer along the measurement axis. The earth's gravity field covers a range from approximately 978 to 983 gal. The sensor system operates in a range of ± 14 gals either side of the earth's nominal gravity value of 980 gal. The full range of the accelerometer output signal is 0 to 994 gal, but limiting the system to the narrower range of 966 to 994 gal provides measurements with increased resolution. Sensor drift rate estimates are calculated by a calibration

procedure that relates sensor measurements to the gravity force. The biased analog signal is converted to a digital signal in a pulse rate converter (PRC) and then transferred to the data acquisition system. The PRC contains a 33 second RC lag filter that attenuates high frequency vertical accelerations created by submarine dynamics with a frequency range outside the gravity measurement range of interest. The low pass filter's function is to prevent saturation of the PRC oscillator.

The stabilized platform isolates the gravity sensor from the roll and pitch dynamics of the submarine motion in order to maintain the sensor-sensitive axis collinear with true local vertical.

The data acquisition group collects, filters, scales, time tags, and records the gravity data measured by the gravimetric sensor group. A calculator controls the data acquisition system by interfacing the system data buffer with the data recording equipment. The buffer receives gravity data from the PRC and accumulates sets of one-second pulses in a binary counter. The gravity pulse counts are proportional to a one-second gravity measurement in milligals. The proportionality factor is a function of the sensor bias, scale factor and drift rate.

In addition to gravity, the gravity measuring system also records disturbing forces due to submarine dynamics with respect to time. In order to accurately account for these

forces, the dynamics of the submarine must be measured. Precise knowledge of the gravity measuring system's three-dimensional position with respect to time is essential to relate gravity measurements to presurveyed reference maps of sea-level gravity versus position. The submarine's navigation system collects the necessary parameters to calculate these relationships. Latitude, longitude, velocity, depth, time and attitude are recorded independently of the gravity measurement system.

In this study, relative gravity measured onboard a submarine will be one of the principal variables examined. As discussed, several disturbing forces will have adverse effects on the signal. The filtering techniques automatically applied by the measuring system may inadvertently remove or distort the signal that is sought in this study. In this study we will examine the usefulness of submarine accelerometer data and whether these effects can be understood and not obscure the signal potentially associated with ocean turbulence.

B. LARGE EDDY SIMULATION MODEL AND THE FROZEN EDDY HYPOTHESIS

The principal objective of this section is to describe the Large Eddy Simulation (LES) model and how it is used in this study. We would like to simulate motion of the submarine through the LES field and develop methods for comparing the model produced data with the submarine observations of velocity and acceleration. The "Frozen Eddy" hypothesis is also

described; a scale analysis is performed which allows a hypothetical submarine to be driven through the LES-simulated convective field, mapping the field by taking "snapshots" of the turbulence field "frozen" in time.

1. LES Model

The LES model has evolved as a very useful tool to help oceanographers study complex geophysical flows. The model is nonhydrostatic and predicts the turbulent velocity, temperature and salinity fields in high Reynolds number flows. Mixed layer and pycnocline processes may be simulated, realistically representing the turbulence that a submarine might experience. The LES simulates the large eddies but parameterizes the smallest eddies. For highly turbulent flows, this model parameterization requires that the grid size falls within the inertial subrange of the turbulence. Smaller eddies are less flow dependent and contain a smaller amount of energy. As eddies become smaller through the turbulent cascade process, they become less dependent on the large scale flow and contribute little to the overall transport of momentum and heat. The parameterization of small eddies serves primarily to dissipate the turbulent kinetic energy of the large scales through the use of a nonlinear eddy viscosity. Moeng (1984) provided the original code for the LES model. Garwood et al., (1994) modified the model for use in oceanic deep convection by adding a prognostic equation for salinity and including the

pressure dependence for the thermal expansion coefficient in the equation of state.

The Boussinesq equations plus heat and salinity budgets are used explicitly to calculate the three dimensional large-eddy velocity (u,v,and w are the easterly, northerly and vertical velocity components, respectively), salinity (S) and potential temperature (θ) fields.

$$\frac{du}{dt}=-\frac{1}{\rho}\frac{\partial p}{\partial x}+fv-2\Omega_y w+\frac{\partial}{\partial x}(K_m\frac{\partial}{\partial x}u)+\frac{\partial}{\partial y}(K_m\frac{\partial}{\partial y}u)+\frac{\partial}{\partial z}(K_m\frac{\partial}{\partial z}u)$$

$$\frac{dv}{dt}=-\frac{1}{\rho}\frac{\partial p}{\partial y}+fu+\frac{\partial}{\partial x}(K_m\frac{\partial}{\partial x}v)+\frac{\partial}{\partial y}(K_m\frac{\partial}{\partial y}v)+\frac{\partial}{\partial z}(K_m\frac{\partial}{\partial z}v)$$

$$\frac{dw}{dt}=-\frac{1}{\rho}\frac{\partial p}{\partial z}+\alpha g(\theta-\theta_o)+2\Omega_y u+\frac{\partial}{\partial x}(K_m\frac{\partial}{\partial x}w)+\frac{\partial}{\partial y}(K_m\frac{\partial}{\partial y}w)+\frac{\partial}{\partial z}(K_m\frac{\partial}{\partial z}w)$$

$$\frac{d\theta}{dt}=\frac{\partial}{\partial x}(K_\theta\frac{\partial}{\partial x}\theta)+\frac{\partial}{\partial y}(K_\theta\frac{\partial}{\partial y}\theta)+\frac{\partial}{\partial z}(K_\theta\frac{\partial}{\partial z}\theta)$$

$$\frac{dS}{dt}=\frac{\partial}{\partial x}(K_s\frac{\partial}{\partial x}S)+\frac{\partial}{\partial y}(K_s\frac{\partial}{\partial y}S)+\frac{\partial}{\partial z}(K_s\frac{\partial}{\partial z}S)$$

$$\frac{\partial u}{\partial x}+\frac{\partial v}{\partial y}+\frac{\partial w}{\partial z}=0$$

Here f is the vertical Coriolis parameter, and $2\Omega_y$ is the horizontal Coriolis parameter. The eddy mixing coefficients ($K_{m,s,\theta}$) are used to parameterize the subgrid scale fluxes that are time and space-dependent.

2. "Frozen Eddy" Hypothesis

The "Frozen Eddy" hypothesis was used for simulation of a submarine driven through a turbulent convective field. The governing premise of this hypothesis is that the speed of the submarine (Us) is large enough so that an eddy appears invariant with time ($\partial w/\partial t$ negligible) and the total derivative (dw/dt) is dominated by the product of the change in vertical velocity along the direction of motion ($\partial w/\partial x$) and the speed of the submarine (equation 2). A physical analogy of this premise would be an ant, moving rapidly through a corn field, would not see any changes in the local field($\partial w/\partial t$); that is, the ant would not see the corn growing due to its own fast speed through the field. Conversely, an ant moving very slowly through the field would see local changes in the field, and the local evolution of the field could not be ignored. Equation (2) governs vertical acceleration experienced by the submarine where x is the horizontal coordinate parallel to the submarine's course and positive in the direction of motion.

$$\frac{d(w)}{dt} = \frac{\partial(w)}{\partial t} + U_s \frac{\partial(w)}{\partial x} \qquad (2)$$

The hypothesis is effective if the local evolution of the velocity field is much less than the product of the speed of the submarine and the rate at which turbulence changes in space.

$$\left|\frac{d(w)}{dt}\right| \ll \left|U_s \frac{\partial(w)}{\partial x}\right|$$

For this scale analysis, τ represents the time scale of the eddies or turbulence and w^* is the vertical velocity scale.

$$\frac{\partial(w)}{\partial t} = \frac{w^*}{\tau}$$

λ_x represents the spatial scale of the eddies or turbulence.

$$\frac{\partial(w)}{\partial x} = \frac{w^*}{\lambda_x} \Rightarrow U_s \frac{\partial(w)}{\partial x} = U_s \cdot \frac{w^*}{\lambda_x}$$

$$\left|\frac{1}{\tau}\right| \ll \left|\frac{U_s}{\lambda_x}\right|$$

h is equal to the mixed layer depth and is the approximate size of λ_x:

$$\lambda_x \propto h \quad \therefore, \quad \tau \gg \frac{h}{U_s}$$

Likely values for mixed layer depth and the speed of the submarine will be used to calculate the ratio of mixed layer depth and speed of the submarine. This scaling factor will be of use for comparison with typical time scales for turbulence.

$$\tau \gg \frac{h}{U_s} \sim \frac{100\ m \rightarrow 2000\ m}{5m/s} \qquad \therefore, \qquad \tau \gg 20\ s \rightarrow 400\ s$$

W^* represents the turbulent velocity scale, which is useful for an approximate calculation of the time scale for turbulence (τ).

$$\tau \gg \frac{h}{U_s}$$

$$\tau \simeq \frac{h}{W^*} \qquad \tau \simeq \frac{100m \rightarrow 2000\ m}{.01m/s \rightarrow .05m/s} \simeq 10^4 s \rightarrow 4x10^4 s$$

The period τ of 10^4s is much greater than 20s, and therefore the assumption that the local changes in the field are insignificant due to the speed of the submarine is a good one. The rate at which turbulence changes with time is so small that the whole picture can be resolved by $U_s(\partial w/\partial x)$.

C. LES MODEL DATA ANALYSIS

The LES model of Garwood et al.(1994) uses a three dimensional domain 2.075km deep(z) with 6.4km on each axis in the horizontal (x and y). The model has 41 vertical levels and a 128 by 128 matrix of evenly spaced horizontal grid points, having a resolution of 50m in the horizontal. Initial sea surface temperature was 3.0C and sea surface salinity was

34.85psu. Horizontal boundary conditions are doubly periodic. Surface condition is slip, with constant wind stress applied; the bottom boundary condition is no slip. The temperature field is freely advected by the buoyancy driven convection. The simulations were run until statistical equilibrium was achieved in each case. The two simulations consisted of a low wind and a high wind case which both had 400watts/m^2 surface heat loss. The LES simulations depict a high latitude area in the winter with deep convection corresponding to a deep 2000m mixed layer. The low wind case (Figure 9) represents buoyant or free convection only, while the high wind case (Figure 10) is a combination of forced and free convection.

In order to make statistical comparisons with actual accelerations observed aboard a submarine a hypothetical massless submarine was driven through the "frozen" LES-computed field at level 3 (125m) and the spectra for the vertical velocity field were computed, Figures (9) and (10). In all LES simulations, kinetic energy is introduced at lower wavenumbers (k). In Figure (9) the spectral energy density (3.8e-03(m^3/s^2) peaks at approximately k= 1.2e-03(1/m). Following the peak, energy begins to drop off with an approximate k^(-5/3) power law spectral shape. Through the inertial subrange, energy cascades from larger to smaller eddies toward higher wavenumbers. Beyond k=6.0e-03(1/m) turbulent energy is dissipated by smaller eddies. The

pronounced energy peak corresponds to a horizontal wavelength of about 1000m which is related to the depth of mixing. The depth of the mixed layer is approximately double the inverse of the wavenumber value (1.2e-03(1/m)) corresponding to the peak energy. Thus, the mixed layer is about 1700m deep due to strong thermal forcing and subsequent free convection. With peak energy at a horizontal wavelength of 850m, this indicates that at approximately every 850m another convective plume would be expected.

The high wind case (Figure 10) has a similar profile with a broad energy peak from k=5.0e-04 to 9.0e-04(1/m) and 4.5e-03(m^3/s^2). In this spectrum, energy is spread out over a larger scale. Due to the added influence of momentum flux caused by stronger winds, more energy is present, evident by the larger area under the curve or the larger integral of the spectrum. In view of this wind driven convective spectrum, observed turbulence data created from similar forcing may display a similar profile, and the energy may assume a larger-scale broad peak energy distribution versus a smaller and more peaked profile than if it were solely forced by buoyancy.

Ignoring the hypothetical submarine's mass and length, the relative acceleration of gravity of the submarine (g'_s) is equal to dw/dt which from the frozen eddy hypothesis can be approximated by $U_s(\partial w/\partial x)$. This yields:

$$g_s = \frac{dw}{dt} \cong U_s \frac{\partial w}{\partial x}$$

The signal from which the spectrum of Figures (9) and (10) came from can be described by f_1=A sin(kx) with A equal to the amplitude of the signal and k equal to the wavenumber. A sin(kx) is equal to w. Once w is differentiated, $(\partial w/\partial x)$=Akcos(kx). This yields:

$$g_s = U_s \frac{\partial w}{\partial x} = U_s Ak\cos(kx)$$

Due to the multiplication of the amplitude (A) by the wavenumber (k) upon differentiation of w, the higher frequencies are more heavily weighted. The LES spectra of dw/dt for free and wind driven convection are depicted in Figures (11) and (12). In both cases peak energy is more than two orders of magnitude less than the w spectra and has shifted slightly to higher wavenumbers. This would indicate that the predominant wavelength of these accelerations is shorter and consequently their frequencies are higher. Due to the larger amount of energy present in the higher frequencies, turbulence should be looked for in this region of an acceleration signal which is analogous to (dw/dt). Thus, the more high-energy high frequency portion of the (dw/dt) spectra

is the suspected range of wavenumbers for turbulence and represents the most significant region of the differentiated signal.

V. ANALYSIS OF SUBMARINE RECORDED DATA

GSS (Gravity Survey System) data from a submarine was provided for this research by the Program Management Office, Strategic Systems Programs in Great Neck, New York. The data was recorded onboard a U.S. Navy ballistic missile submarine that was conducting operations 200 to 300 nautical miles east of Cape Canaveral, Florida in the summer of 1994. Details concerning the submarine's operations were not made available due to classification considerations, but are not required for this initial study. We had specifically requested gravity data, but data from the Submarine's Inertial Navigation System (SINS) and a keel depth sensor were also included.

A. NAVIGATION DATA

The navigational data extends for a period of 5.8 days with a sampling rate of 2 seconds (Δt=2s). A time-integrated three component accelerometer measured east(u), north(v), and vertical(w) velocities as part of the SINS. These terms represent the ship-to-ground inertial velocity components and were measured in feet per second (ft/s). Correction factors for the accelerometers are unknown. Velocity of the submarine with respect to the water was recorded by two sensors located fore and aft on the submarine. A pressure sensor calibrated to correct for position of the keel measured how much water was overhead to record keel depth data in feet (ft).

To find turbulence, the mixed layer is a good location due to momentum and heat fluxes driving convection in that region of the ocean. As displayed by the keel depth record (Figure 13a), the submarine operated for short time segments at standard depth 1 (SD1) which is located in the mixed layer and for longer time segments at standard depths 2, 3 and 4. Ideally, submarine data from the winter time at higher latitudes would most likely show evidence of turbulence. Never the less, the data provided gives a representative "background" acceleration field to compare with LES predictions. Based on the XBT soundings (shown later) and climatology a mixed layer with appreciable depth was not present and the submarine-recorded data was mostly at depths in the thermocline, below a shallow mixed layer. Data from both a turbulent source and a nonturbulent source would be useful to contrast and compare.

Figure 13b depicts the SINS vertical velocity (w) converted to meters per second (m/s) for the entire record. This figure also displays the submarine's speed and keel depth converted to m-k-s units for the entire record. With a 2 second sampling rate, a very large amount of data was recorded. Out of the three components of velocity the SINS provides, w was of primary interest. The vertical velocity (w) reflects the submarine's vertical fluctuations in position. It is a measure of both the flow around the submarine and what the submarine itself is experiencing do to its own mechanical input.

1. Vertical Velocity Data (w)

Four time segments of the data, in which the submarine maintained a relatively constant depth, were extracted to examine in detail. The segments were standard depth 1 (SD1, very shallow and probably within the mixed layer), standard depth 2 (SD2, shallow and below the mixed layer), standard depth 3 (SD3, mid-depth and below SD2) and standard depth 4 (SD4, deep and below SD3). This segmentation of the data improved management of the very large amount of data, and it enabled the comparison of different regimes. It is possible that the submarine transited an area with some type of active turbulence forcing which could then be contrasted with transit areas of known stably stratified water. Once the data segments were extracted, several variables were analyzed.

Submarine speed versus time, vertical velocity (w) versus time and w versus distance for all four standard depths are displayed in Figures 14, 15, 16 and 17, respectively. Since the speed of the submarine varied from near zero to about 8m/s, w for each case is shown as a function of distance to eliminate the speed of the submarine as a source of variability in the signal. When w is plotted versus distance (Figures 14c, 15c,16c and 17c), the variability of the fluctuations in amplitude may be due to a variable reaction of the submarine to speed through the water. As the submarine moves faster, its response to steering or to external disturbances appear to be faster than

when the submarine is traveling more slowly. The submarine appears to behave dynamically different at different speeds as reflected in the fluctuations in the amplitude of w. Examining the w time series reveals that SD4 has a lower frequency signal relative to SD3, and SD3 has a lower frequency signal relative to SD2, and SD2 has a lower frequency relative to SD1. The higher frequency signal and also much higher amplitude of SD1 may be influenced by a combination of surface gravity waves, internal waves and turbulence. As the depths increase and surface effects have less of an influence, the frequency of the signals for SD2, SD3 and SD4 all decrease, with SD4 exhibiting the lowest frequency. These frequency characteristics are supported by their respective spectra. Figures 18, 19, 20, and 21 display the windowed power spectral density versus wave number (k) for SD1 through SD4, respectively. These plots show when each depth region begins to experience high frequency energy, possibly near the inertial subrange. SD4 appears to enter the inertial subrange at approximately 1.0e-07w^2, SD3 at 1.0e-06w^2, SD2 at about 1.0e-05w^2 and SD1 enters the subrange at about 8.0e-03w^2.

2. XBT and Climatology Data

Climatological data was obtained for a large geographic area that encompasses the operating region of the submarine off the east coast of Florida. Comprehensive Ocean/Atmosphere Data Set (COADS) climatological sea surface temperatures ranged from

29.2C at the approximate western extent of the operating area to 27.8C at the eastern extent for July. Temperature profiles from Levitus climatology were also examined and showed very shallow mixed layers in this region with stable stratification below. The climatological winds were light and variable.

The expendable bathythermograph (XBT) data (Figure 22) taken from two different locations within the submarine's operational area, during the time of the submarine operation, depict shallow mixed layers and show that SD1 may be in or just below the mixed layer. Based on these XBT data the region has a variable thermocline with a stably stratified mid-depth region which may correspond to SD2 and SD3. Buoyancy frequency (N) is a function of temperature and salinity, but temperature dominates. SD3 would have the highest N. SD1's large amplitude fluctuations depicted in Figure 14c may be due to turbulence within the mixed layer. SD2's amplitude fluctuations (Figure 15c) may be due to internal wave energy from the mixed layer above. SD3's amplitude fluctuations (Figure 16c) might be expected to be the smallest out of the four standard depth segments due to possessing the greatest stability (highest N), but it does not appear so. Of the four different segments, SD4 displays the smallest amplitude fluctuations (Figure 17c).

B. GRAVITY DATA

The gravity data, for the same time period consists of data from two separate gravity-measuring accelerometers (gma)

and "gravity anomaly from map" (G_{map}). The gma measurement consists of the earth's gravity plus any accelerations the submarine experiences plus sensor noise. Figure 23a displays the entire gravity record (gma1) in units of milligals (mg). The gravity data was sampled at 36 second intervals ($\Delta t=36s$). Gravity anomaly from map, provided to the submarine by Naval Oceanographic Office, is the earth's true gravity field and is shown in Figure 23b. The submarine community's primary interest in gravity has been for navigational purposes. Typically the navigation information is extracted from a lower frequency signal with consistent trends that may reflect ocean bottom topography with significant gravity structure. The interest of this study was the higher frequency signal that may contain the vertical fluctuations of the submarine on a more rapid time scale of minutes and shorter. This can be seen in Figure 23c which is the recorded gravity signal minus the earth's true gravity field (g_{map}).

The gravity data corresponding to the SD2 segment was chosen for further examination. The gravity record for SD2 (Figure 24a), showed a distinct rise in gravity with a prominent peak followed by a dropoff over a 200 minute time period. This long wavelength feature is a depiction of the real gravity field as the submarine transited over a topographic feature. With the earth's gravity (Figure 24b) subtracted, the peak is removed and the remaining high frequency signal (Figure

24c) consists of accelerations experienced by the submarine.

As discussed earlier, in the previous turbulent convection experiment by Schott et al., (1993), the variance of vertical velocity (W'^2) was used as an indicator for turbulence. In those studies the vertical velocity data was recorded by stationary ADCP's. In this study three different instruments, gma, SINS and keel depth sensor, all measure vertical changes, recording either acceleration, velocity or depth, respectively. This provides flexibility and a good cross comparison capability. Any of the three could be integrated or differentiated to compare the different signals. Noise and other signal sources could be evaluated and compared with the gravity signal to establish its potential to detect turbulence.

C. ANALYSIS AND COMPARISON OF OBSERVED W AND GRAVITY DATA

Both the gravity signal and the vertical velocity signal exhibit fluctuations which were discussed earlier in Section IV.A. These forces imposed upon the submarine by the environment, the submarine's own hydrodynamics interacting with the environment and the human input (e.g., planesman steering) are all factors that can mask the desired signal reflecting the presence of turbulence. One method to help reduce the influence of these effects was to locate segments of constant submarine speed. SD4 was chosen to make the comparison of the signals produced from the three different instruments. It was chosen because its signal looked the most uniform in time. An

approximate constant speed section was extracted from SD4 (Figure 17). Two approaches were available to compare the three measured signals. The first was to integrate with respect to time the gravity signal to compare to the vertical velocity signal and then to integrate both signals for comparison with the keel depth signal. The second method was to differentiate with respect to time the keel depth signal for comparison with the vertical velocity signal and then differentiate both of those for comparison with the gravity signal. In order to eliminate the necessity to detrend the signal and to reduce filtering, which could create aliasing, the differentiation method was chosen. Figure (25) displays the time differentiated keel depth (dkeel/dt) in the lower plot and the SINS vertical velocity signal in the upper plot. The signals had a 0.75 correlation with the more distinctive peaks matching up fairly well.

Figure 26b displays the second time differentiation of the keel depth (d^2keel/dt^2), 26c displays the differentiated vertical velocity (dw/dt) and 26a displays the gravity signal, gma1. The noticeably longer period of the gravity signal is due to the 36 second sampling rate. The "boxy" look of the keel depth signal evident in the differentiated signals is due to discretization. The sensor may not be very precise and the signal has a truncation factor which causes incremental jumps. Because this is indicative of a less accurate measurement, this

signal was not used for correlating with the gravity signal.

To improve the comparison of signals that were sampled at different rates, dw/dt was averaged every 18 points and subsampled every 36s (Figure 27c). A correlation of 0.38 between the differentiation of smoothed dw/dt and the gravity signal (Figure 27a) was found. In addition to the low correlation, the gravity signal amplitude is two orders of magnitude less than the SINS dw/dt signal. The gravity signal may be subject to unspecified damping and/or noise. In the BGM-3 gravimeter system the front end of the PRC contains a 33 second RC lag filter to attenuate high frequency vertical accelerations caused by submarine hydrodynamics with a frequency range outside the range of the desired gravity measurement (Mays and Falchetti, 1978). This may indicate that the high frequency signal that is desired for this study is being filtered out. The gravity measuring accelerometers have similar filtering to the BGM-3 gravimeter (Epstein, personal communication, 1995).

The power spectral density (w^2) versus wave number was computed for all four standard depth segments. Figures 28 and 29 display the spectrum for SD1 and SD4 respectively. A large general increase in energy (peak), an energy decrease or dropoff and the wave number area were all similar for standard depths 2,3 and 4. These spectra may represent a mixture of waves and turbulence. SD1 displays two large peaks of energy at

k=5.0e-03(1/m) and k=5.0e-02(1/m). This signal displays the largest amount of energy and is influenced by surface effects. SD4 appeared to have an energy peak at approximately k=2.0e-02(1/m). To remove noise and large scale features and to magnify potential areas of interest, 19 Hanning windows were applied to SD1 (Figure 18) and SD4 (Figure 21). A -5/3 and a -3 slope line are plotted for comparison with the data. The large peaks displayed in Figures 18 and 21 may represent the wavenumbers where turbulent energy is being introduced. This energy input region may be related to surface gravity waves and turbulence in SD1; it may be due to internal waves and turbulence in SD2, SD3 and SD4. XBT and climatology data discussed earlier depict a well stratified column through mid-depths. This would suggest the presence of more internal waves for SD2 and SD3 which require a restoring force that would not be present under unstable conditions. The k^(-3) power law spectral shape describes a region that bridges the energy input or turbulent acceleration zone to the inertial subrange region described by the k^(-5/3) power law spectral shape (Turner,1973). SD1, SD3 and SD4 profiles show an approximate fit to the -3 slope line. The k^(-3) power law spectral shape identifies the buoyancy subrange of middle size eddies which are quasi two-dimensional because of the suppression of vertical motions by stability. In the inertial subrange (high wavenumbers) eddies do not feel the static stability directly,

are three-dimensional and conform to the $k^{(-5/3)}$ power law spectral shape (Stull,1988). It is this region where an energy cascade from small to large wave numbers takes place in turbulent flow.

Kolmogorov's theory of 'local similarity' is based on high Reynold's number flows; and although this data was recorded in an area that did not show a strong turbulent signature, the spectra for all the depth regions show an approximate fit to either one power law spectral shape or the other. The peak of energy in the energy input region may be due to energy producing sources mentioned or may possibly be due to mechanical input from the submarine. There appears to be a cascade of energy toward higher wavenumbers which would indicate that some type of turbulent energy may be present in the water creating this signal. The local similarity theory is based largely on controlled lab conditions whereas real spectra such as these would be expected to contain waves at several wavelengths. The resulting spectra would be complex and would be a function of the relative strengths of the different waves (Turner,1973).

VI. COMPARISON OF OBSERVED AND SIMULATED DATA

The submarine data analyzed here provides a measure of the background accelerations that a submarine might experience in a relatively stable, non-turbulent ocean. It was not from high latitudes, nor was at a time of seasonally strong winds and cooling when turbulent convection is strongest. Thus, this data represents a reference background level of motion that a submarine will experience as it transits through a stable body of water with little or no turbulent signature. On the other hand, the LES model data represents strong turbulence generated by strong thermal and momentum fluxes that would be anticipated in a high latitude region in the winter.

In the free convection case (Figure 9) the maximum energy peak near k=1.2e-03(1/m) and 3.8e-03(m^3/s^2) corresponds to maximum energy peaks near k=5.0e-03(1/m) and 6.0e-02(m^3/s^2), and k=5.0e-02(1/m) and 6.0e-02(m^3/s^2) in SD1 (Figure 28). The maximum energy peak in Figure 9 also corresponds to the peak at k=3.5e-03(1/m) and 1.0e-02(m^3/s^2) in SD4 spectrum of w from the submarine's INS (Figure 29). The peak and the general trend of energy density distribution for the spectra of the observed vertical velocity is largest for SD1 because it is in or just below the surface mixed layer, but the peak energy of the observed vertical velocity spectra for all standard depths exceeded the LES-predicted convection intensity at scales less

than 400m. At scales larger than 400m the LES-predicted convection intensity (Figure 9) was significantly greater than the observed vertical velocity spectra (Figures 28 and 29). This establishes a distinctive spectral gap with observed signal energy exceeding model generated intensity for scales less than 400m and model generated intensity exceeding observed signal energy for scales greater than 400m.

Turbulence can and often does exist below the mixed layer, such as shear-generated turbulence and breaking internal waves. A submarine operating in a deep wintertime mixed layer has a greater probability of recording a strong turbulent signal that can be detected. SD1 is located in the shallow mixed layer which is probably not under the influence of strong turbulence, but its signal generates the largest peaks of energy (Figure 28) which may contain turbulence.

The mixed layer for the LES was about 2000m deep. If the mixed layer were shallower (e.g., 200m) the energy peak would be less and shifted an order of magnitude toward higher wave numbers. This would in effect shift the peak energy into the noise of the submarine-observed data signal and close the spectral gap. Although still unproven, the signal from this standard depth may be influenced by surface effects such as swell, currents, internal waves or by turbulence. Although the sum of all the energy input from both the submarine and the environment in a shallow region make identification and

extraction of the turbulence signal very difficult in the shallow mixed layer, the submarine could be an excellent tool for observing and monitoring the most significant deep oceanic convection such as in the polar and subpolar seas in the wintertime.

VII. CONCLUSIONS AND RECOMMENDATIONS

One of the key aspects of this study was to gain useful oceanographic data from submarine instrumentation that is designed for purposes other than turbulence detection. This information was recorded without altering normal operations of the submarine. This method would enable collection of data by submarines following patrols that spanned the world's oceans, supplementing greatly the infrequent science-designated cruises. The INS appears to be the key instrument for this purpose. It is the heart of the submarine's navigation system and continually records data at a high sampling rate; it appears to be significantly less damped than the gravimeter signal which is two orders of magnitude weaker for the required frequency range. The gravimeter data recorded by the submarine was significantly damped and filtered resulting in a significant loss of signal that may have otherwise included acceleration attributable to ocean turbulence. The gravity data was also sampled at a slower rate (Δt=36s) than the INS vertical velocity data (Δt=2s). Due to the larger volume of information and the better quality of the INS signal, it could more reliably include the turbulence signal sought.

The accurate composition of the signal from the observed submarine data with regard to noise sources, energy input and

submarine operating signature is unclear. Whether turbulence or surface and internal wave motion was detected is also unclear. Further investigation utilizing filtering techniques must be employed. Information pertaining to submarine hydrodynamics would be valuable for gaining an understanding of how and why the submarine reacts to different environmental factors such as variable stratification, turbulence due to convection, and mesoscale phenomena such as fronts and eddies. Further knowledge of the INS, the extent to which its operating signal is damped and other pertinent characteristics of the system should be researched. The more information that can be accessed regarding extraneous input to the submarine recorded signal will increase the effectiveness of filtering with the goal of accurately distinguishing between turbulent acceleration and ship operating acceleration.

The submarine data may have been occasionally collected in a shallow mixed layer, but the vessel predominantly operated below the mixed layer. A significant spectral gap existed between the LES-predicted turbulence signal and the spectra of the vertical velocity for all standard depth segments. For scales less than 400m the spectra of the vertical velocity for all standard depth segments exceeded the LES-predicted convection intensity, and the opposite was true for scales greater than 400m. This would indicate that the background accelerations

attributable to vessel propulsion, hydrodynamics and surface effects during normal operations should not mask the accelerations it would experience if transiting a region of strong oceanic convection. Thus, the submarine could provide copious amounts of observed data with a distinguishable turbulence signal.

The spectrum of SD1 that may have been in the shallow mixed layer exhibited the largest energy peaks and thus the largest spectral gap. Whether the submarine experienced a significant turbulent signal while operating at depth SD1 cannot be ascertained due to the many contaminating sources of submarine motion that can influence the signal and the uncertainty of the total composition of the observed signal. The data from below the mixed layer at depths SD2, SD3, and SD4 were useful in establishing a background operating signal. This background signal would be representative of a nonturbulent, quiescent summertime ocean with no significant momentum or thermal fluxes. The data for depth SD3 were particularly suitable for this purpose because the operating signal has less potential turbulent input from environmental sources than does SD2, and this segment of the water column is most stably stratified as depicted by the XBT profiles. The SD3 signal also represents a baseline operating signal for the submarine, containing signal input due to the submarine propulsion and hydrodynamics under presumed normal

operating conditions. With an established background signal, comparisons can be made with additional future submarine recorded data from the same type of platform. It will be important to obtain data from a high latitude winter time environment to increase the probability of receiving information that may contain strong turbulence. A set of corresponding submarine expendable BT's or CTD profiles from a co-located surface vessel is desirable for correlation with the established background accelerometer signal. The spectral gap similar to that which was evident between the LES turbulence signal and all four standard depth's spectra of w may then be verified. The next step will be to design a filter to remove as much noise and other non-turbulence sources as possible. Upon completion of this procedure, the processed signal can be correlated with the LES turbulence signal with a high correlation indicating that turbulence could be present. The magnitude and direction of the turbulence could then be determined from the processed w signal.

Many aspects of submarine operations are considered sensitive, and close coordination with data sources will have to be maintained to ensure proper handling. Location of the significant cases of oceanic turbulence will be of great scientific and operational navigational importance. With magnitude and location of the turbulence fields determined, mapping of large sections of scientifically and operationally

important bodies of water can be accomplished. If supplementary information such as XBT and CTD data can also be obtained for the operating area and time frame, potential turbulence-producing mechanisms can be examined. This information could provide valuable insight into poorly understood convection generation theories that lack observed data.

The Strategic Systems Programs Office and the Arctic Submarine Laboratory have been excellent sources for data and technological support. The Columbia University Lamonth-Doherty Earth Observatory is a potential source of acceleration data and should be pursued as an additional source of information.

APPENDIX

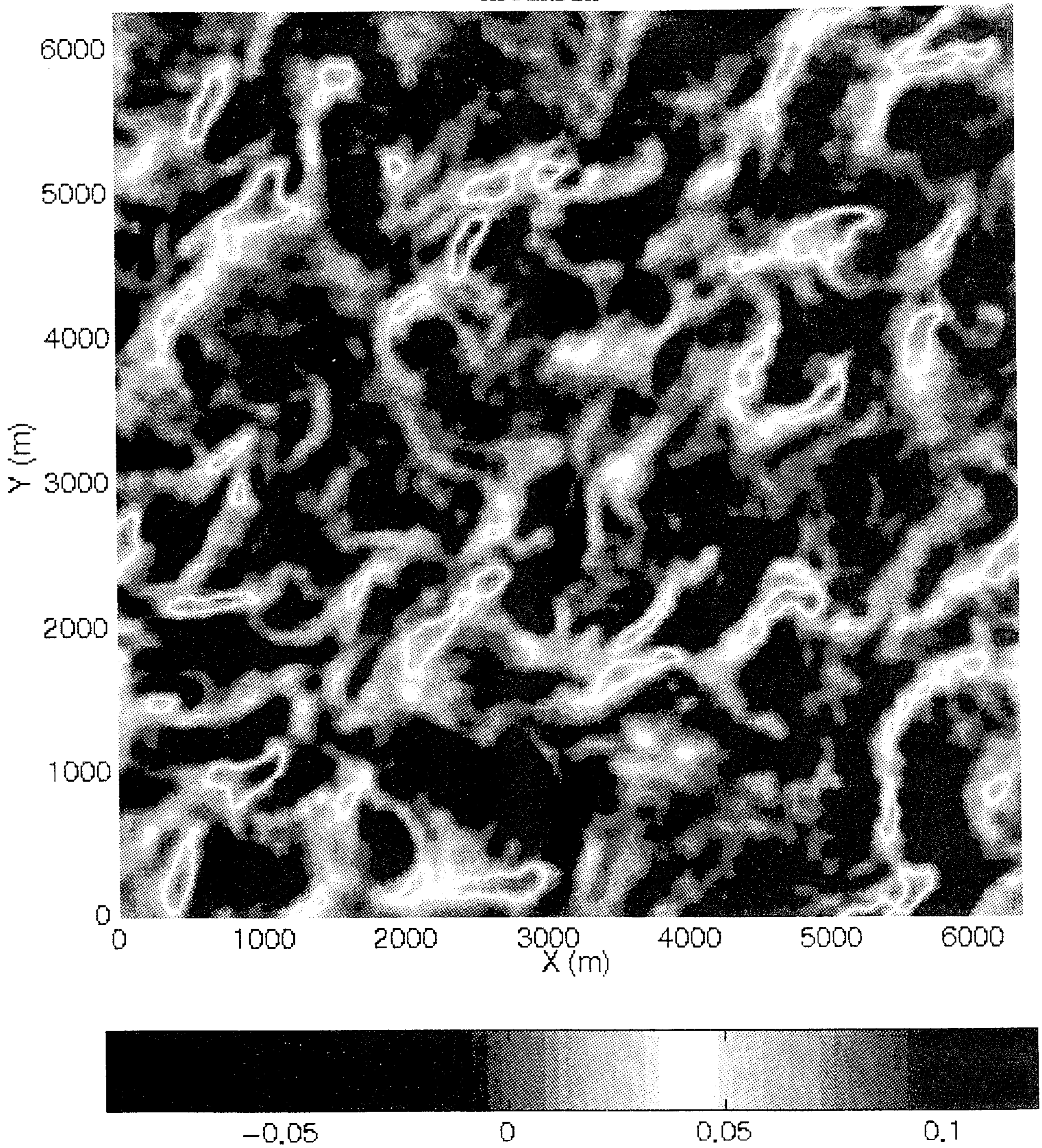

Figure 1. Vertical velocity as a function of X and Y, from the LES model at 125m depth at an instant in time.

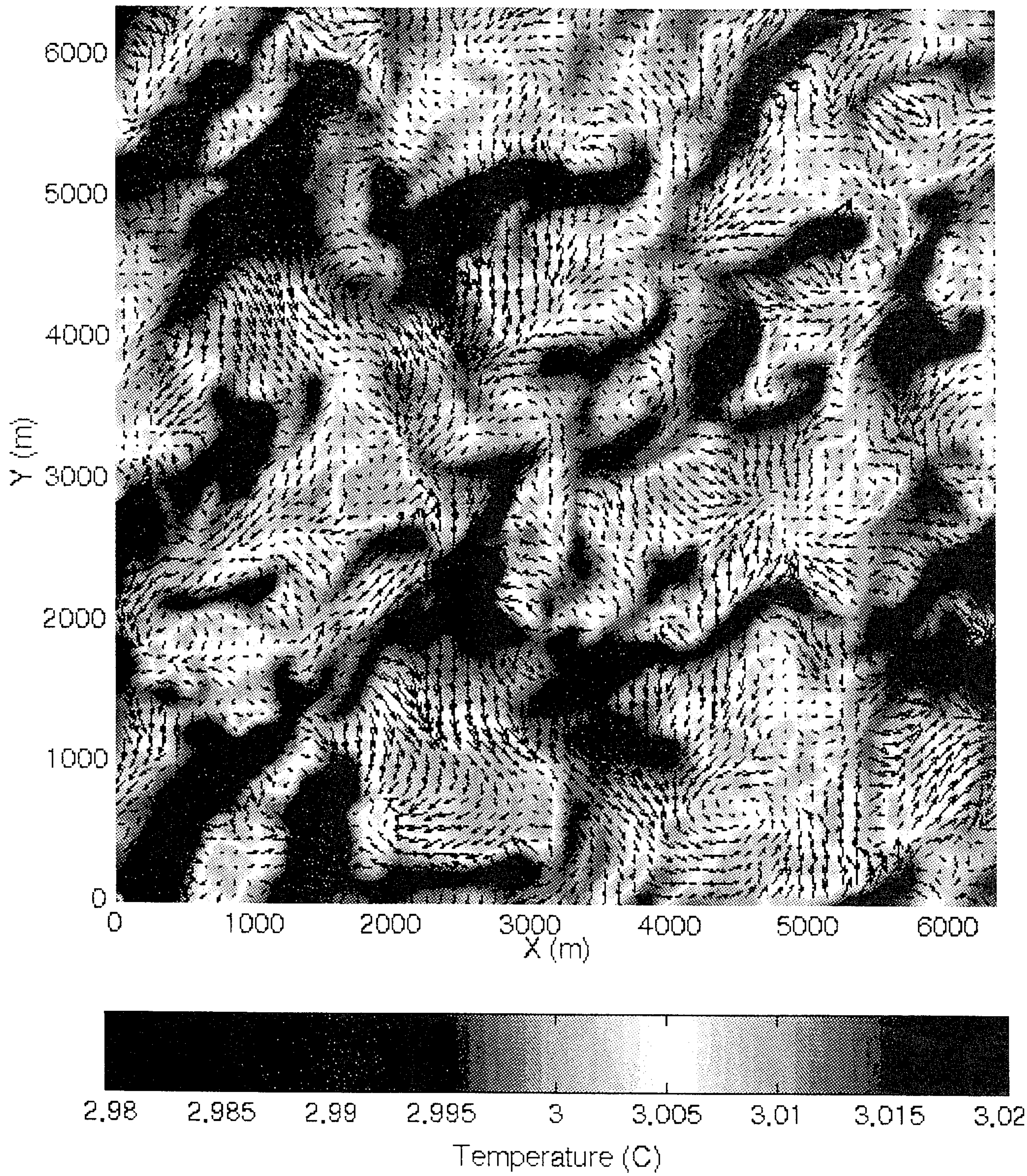

Figure 2. Same as Figure 1, except for temperature and horizontal velocity.

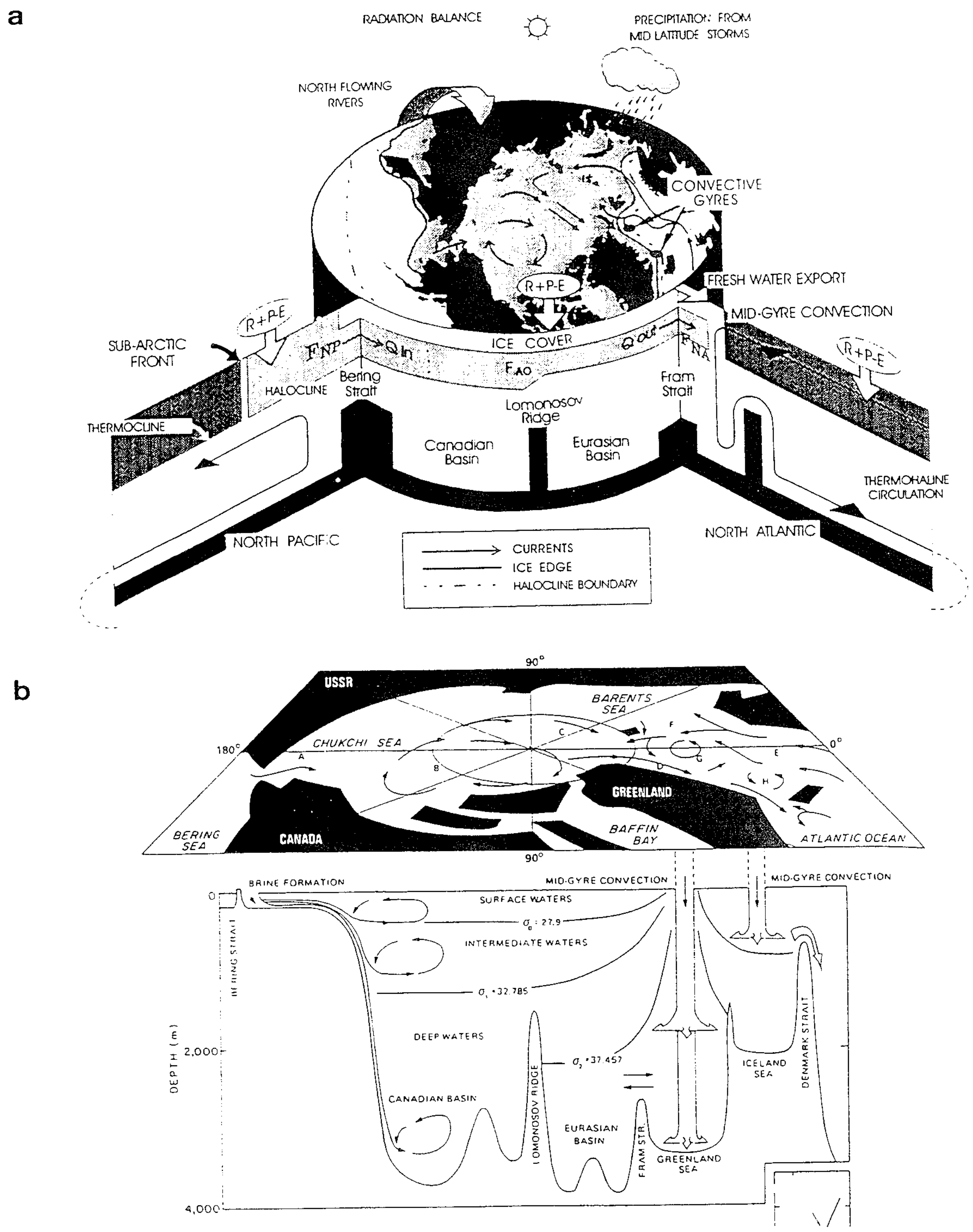

Figure 3. (a) Schematic of Arctic Ocean climate connections. Shaded ovals indicate the present sites of convection in the Greenland and Iceland Seas (from Aagaard and Carmack, 1994). (b) Schematic circulation and water mass structure in the Arctic Mediterranean (from Aagaard et al., 1985).

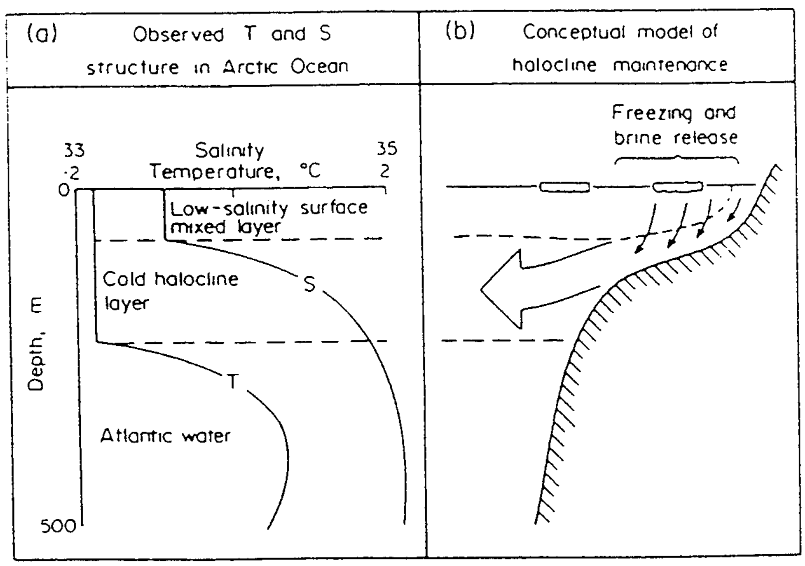

Figure 4. Schematic representation of the temperature (a) and salinity (b) structure in the upper Arctic Ocean and its maintenance (from Aagaard et al., 1981).

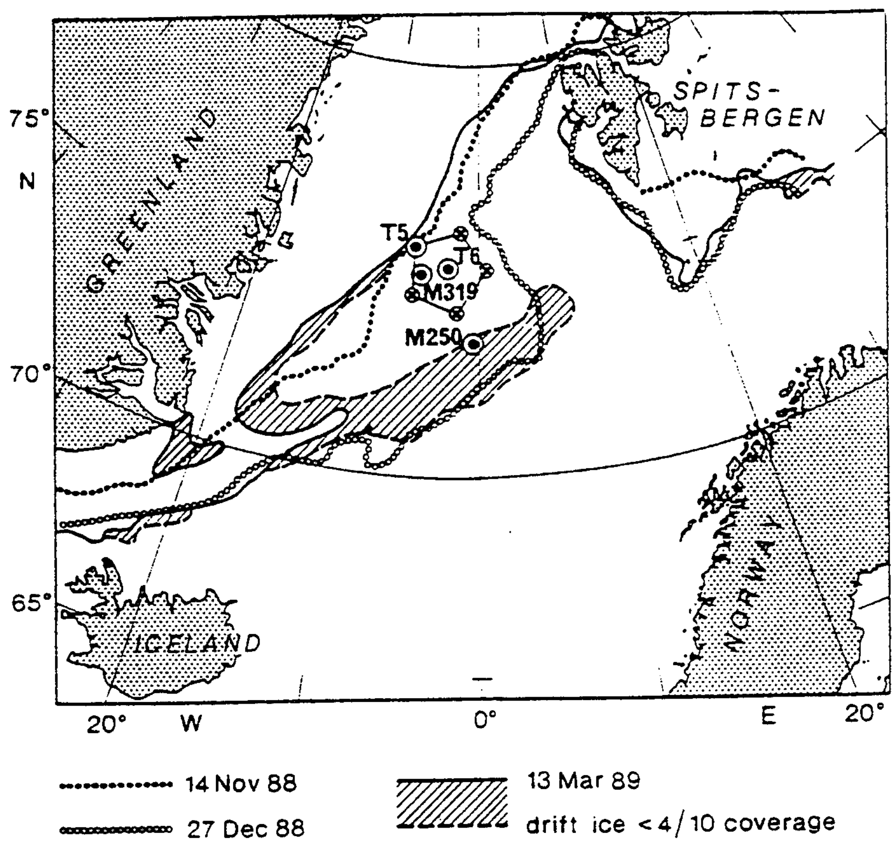

Figure 5. Locations of marginal ice zone during winter 1988-1989 and of ADCP moorings. (from Schott et al., 1993)

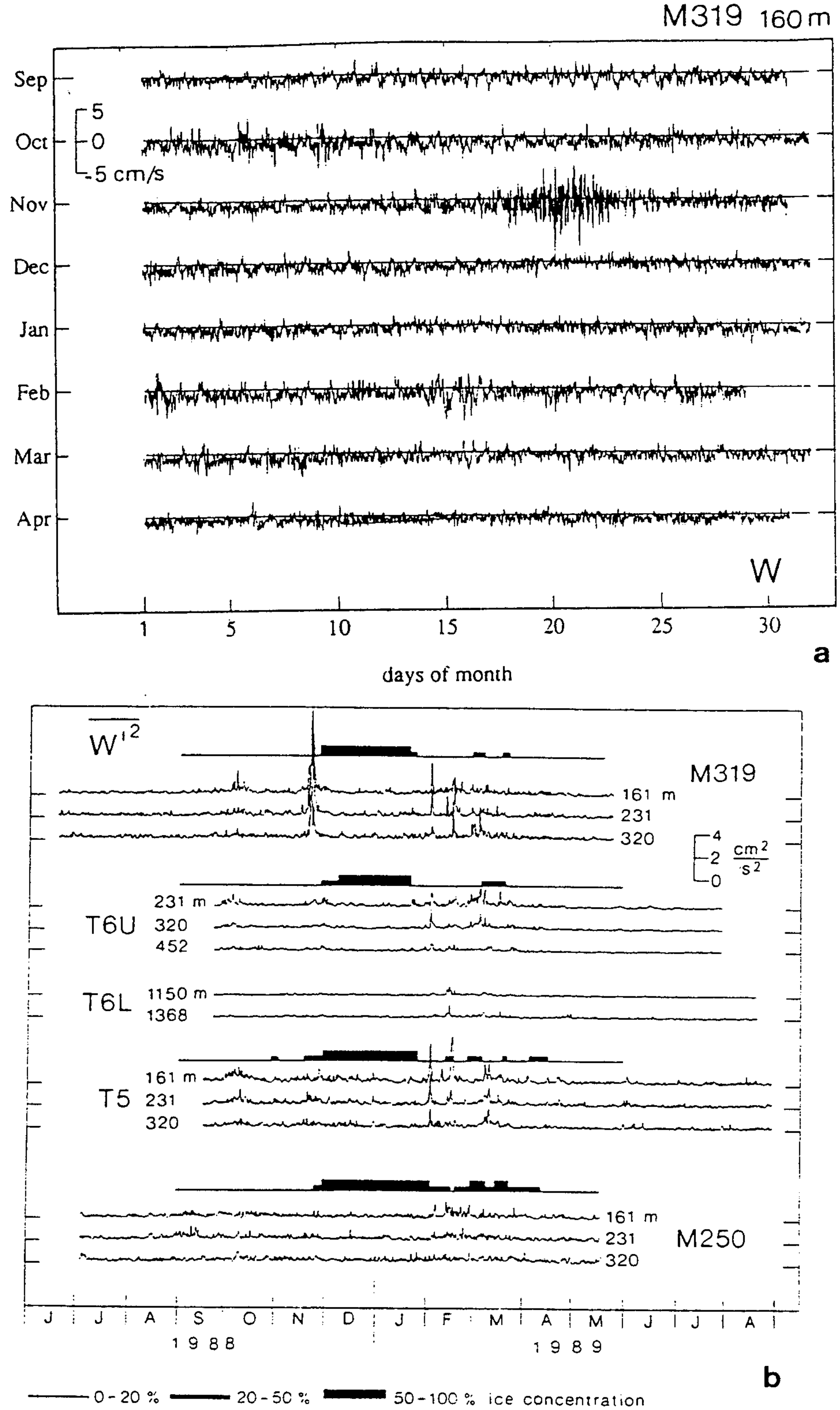

Figure 6. (a) Time series of half-hourly vertical ADCP currents during September 1988 to April 1989. (b) Band passed variance of vertical velocity for several depths of all 5 ADCPs. Ice coverage indicated by bar graphs. (from Schott et al., 1993)

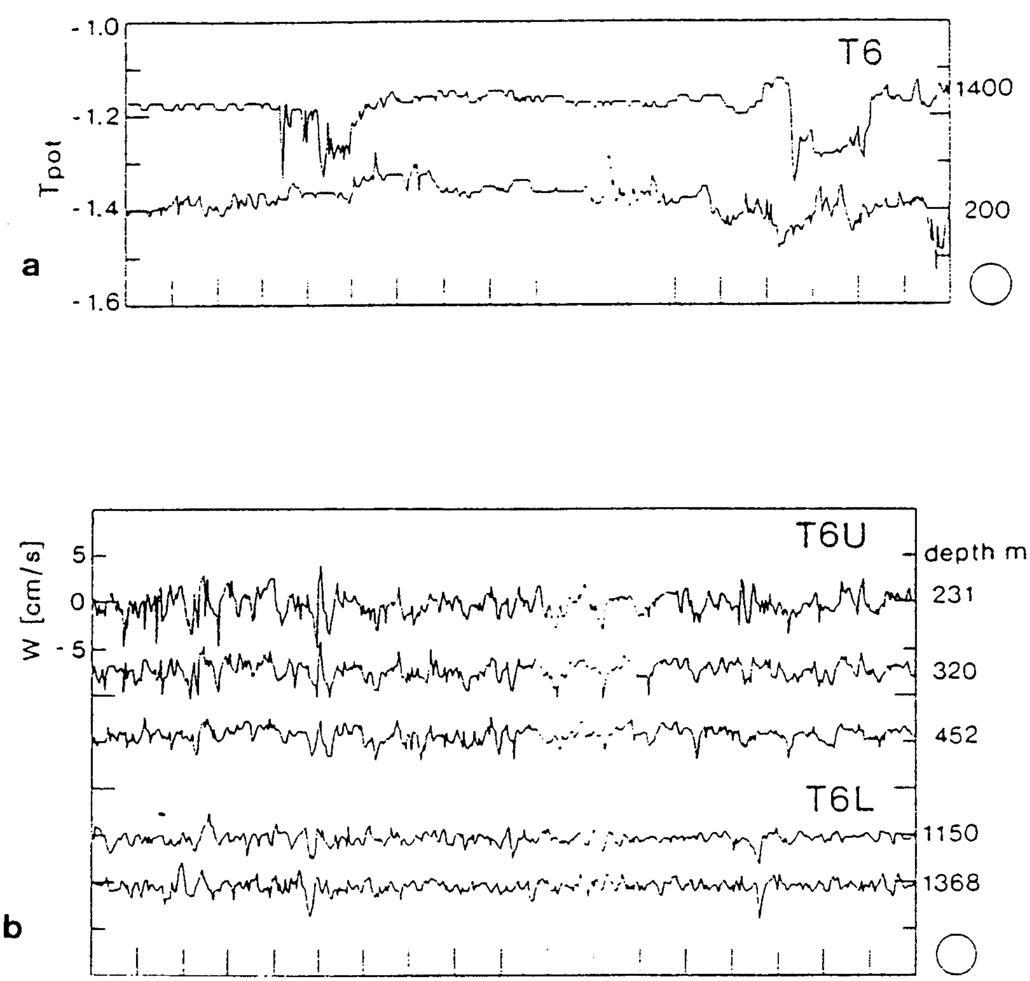

Figure 7. (a) Potential temperatures recorded by ADCPs at T6U and T6L. (b) Vertical currents from several depths at position T6 during March 2-20 (from Schott et al., 1993).

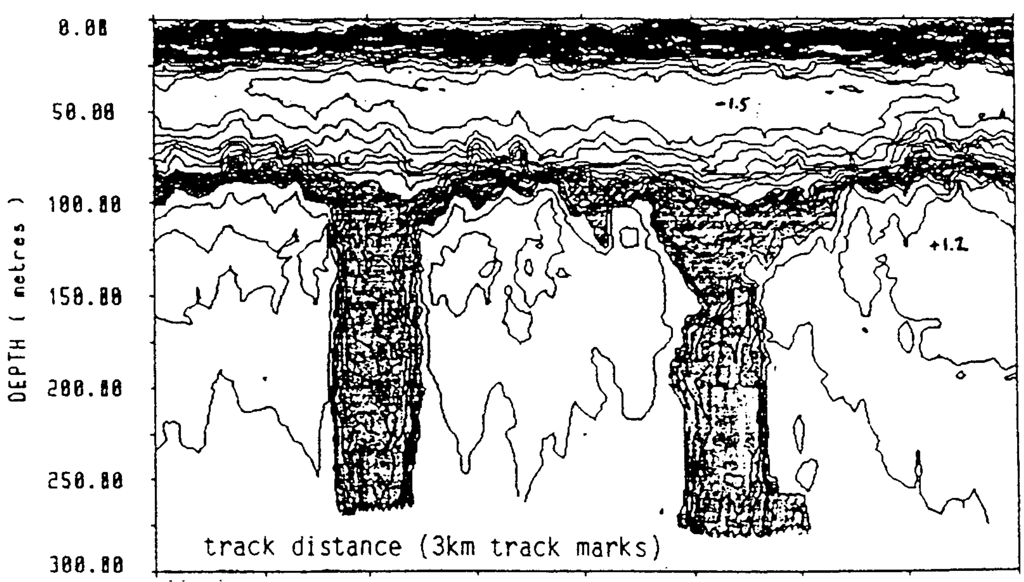

Figure 8. 3km wide vertical cold structures. The contours represent the temperature field from thermistor chain data. (from Scott and Killworth, 1991).

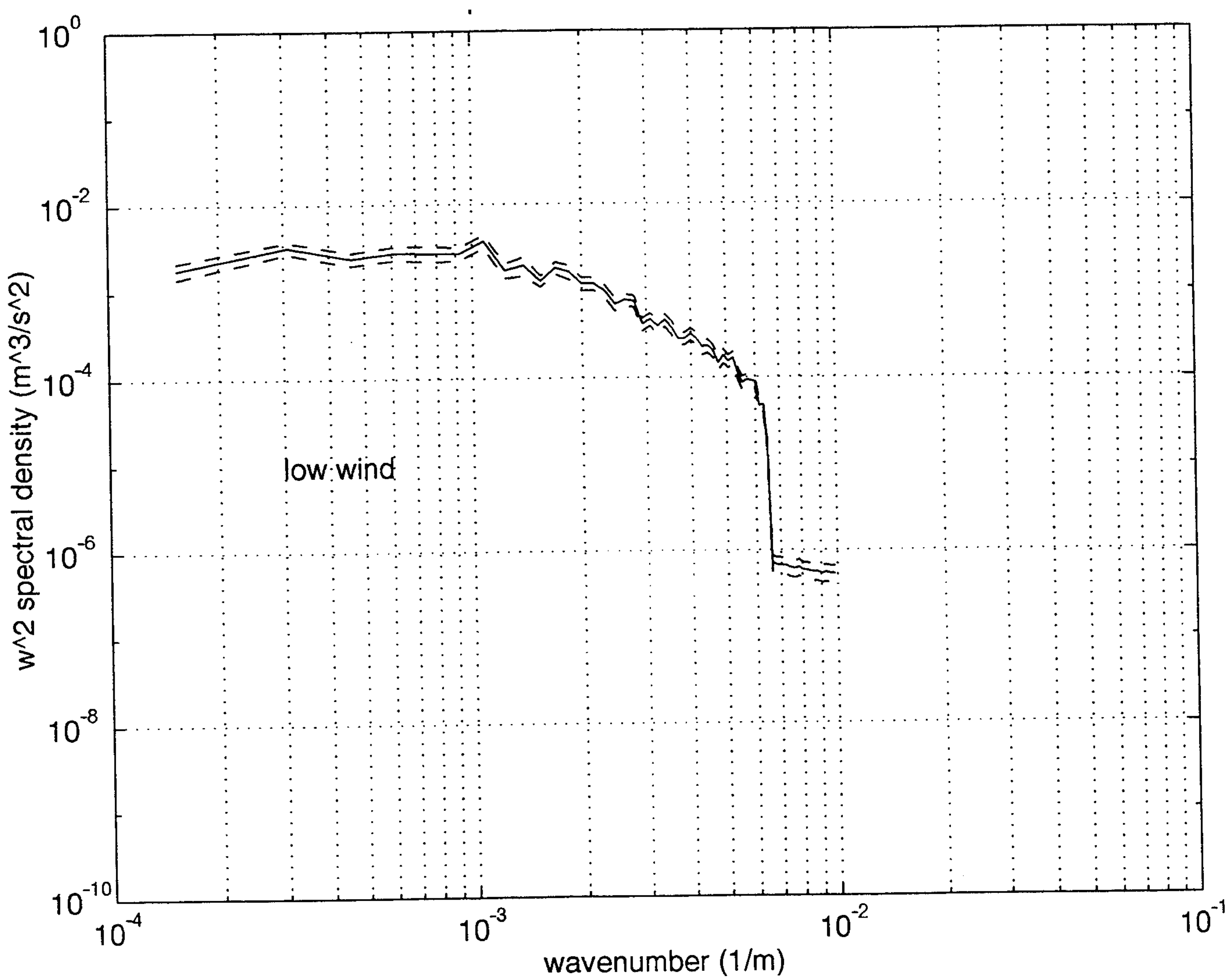

Figure 9. Spectrum of w from LES Model, Level 3. w^2 spectral density versus wavenumber for the low wind case.

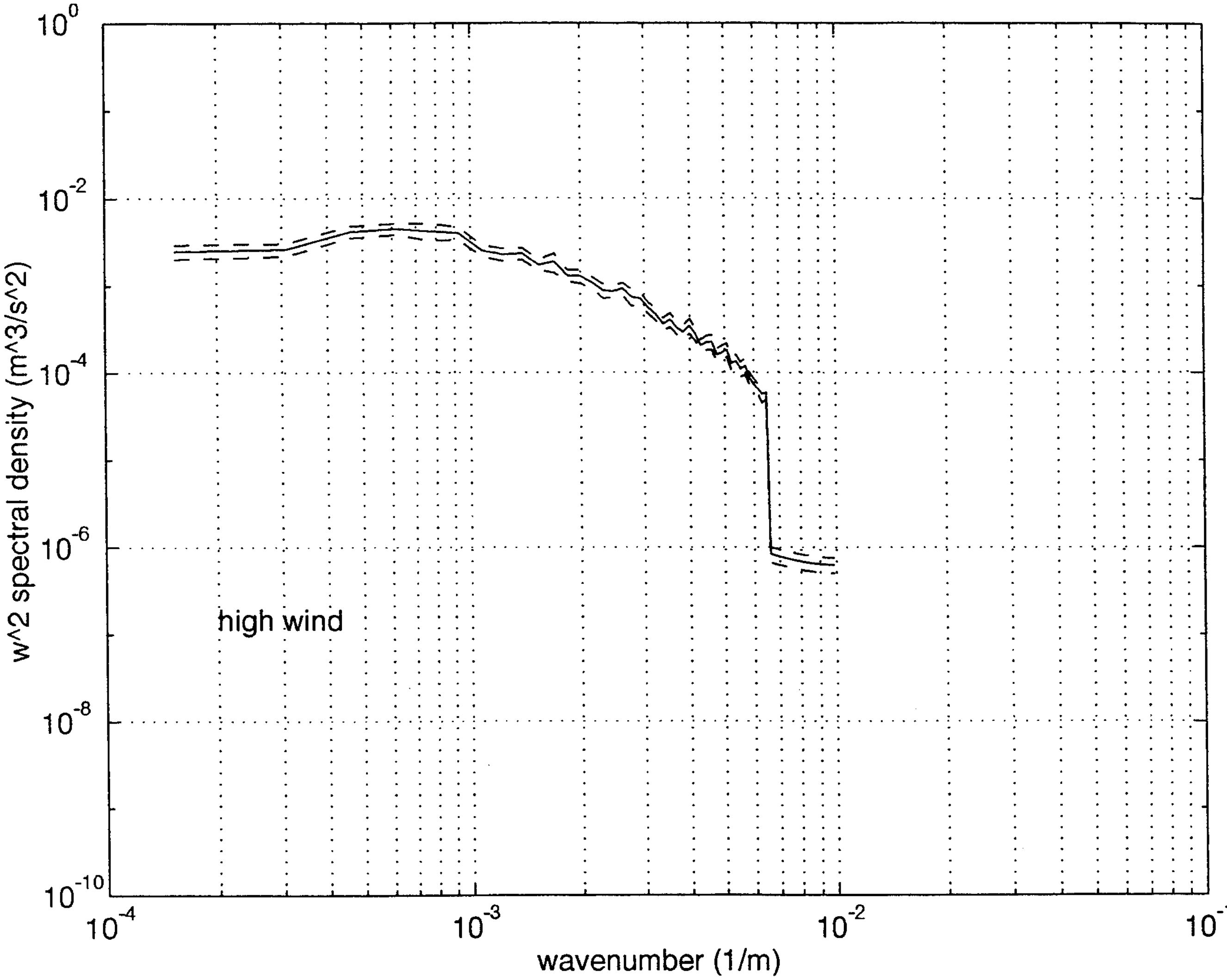

Figure 10. Spectrum of w from LES Model, Level 3. w^2 spectral density versus wavenumber for the high wind case.

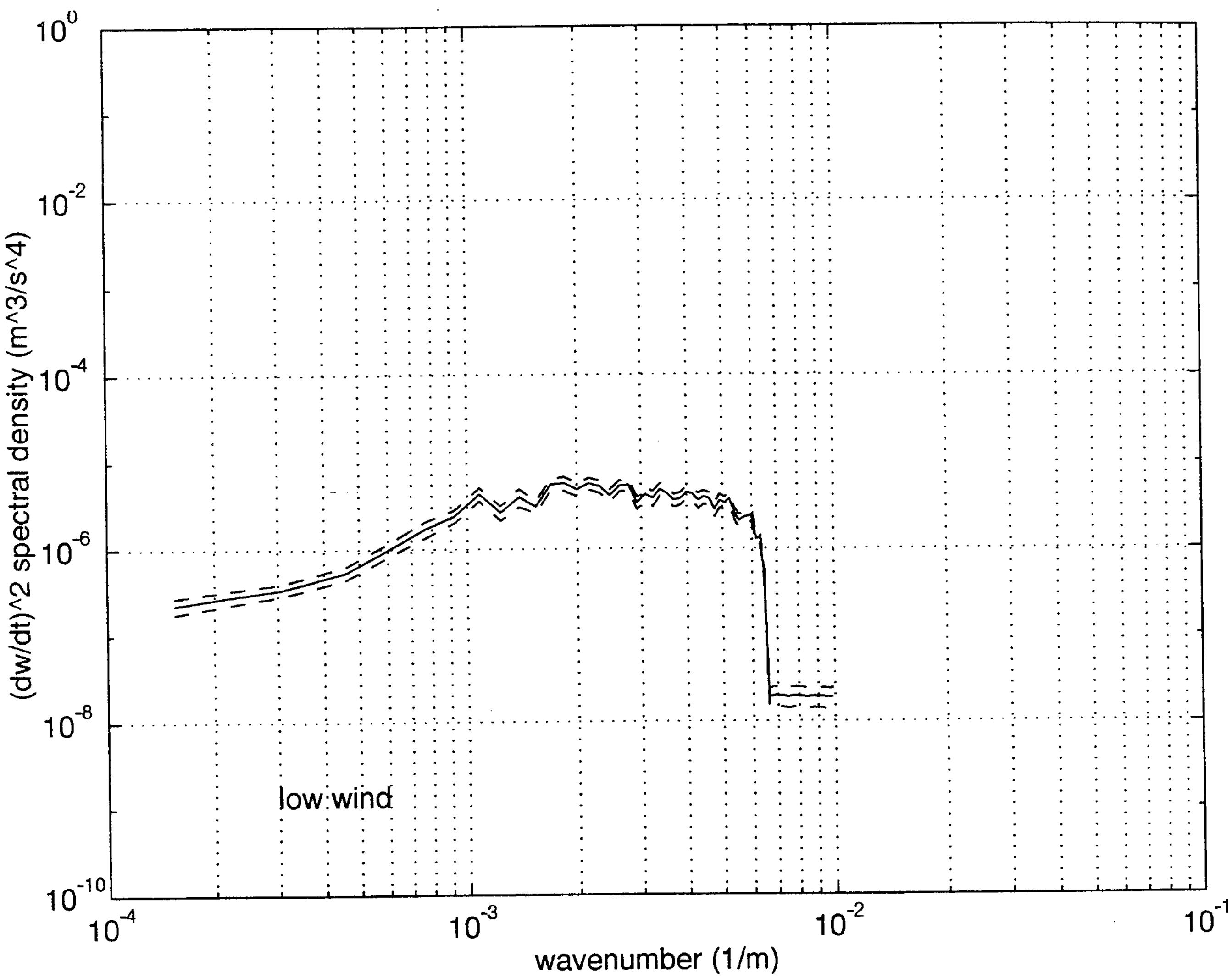

Figure 11. Spectrum of dw/dt from LES Model, Level 3. (dw/dt)^2 versus wavenumber for the low wind case.

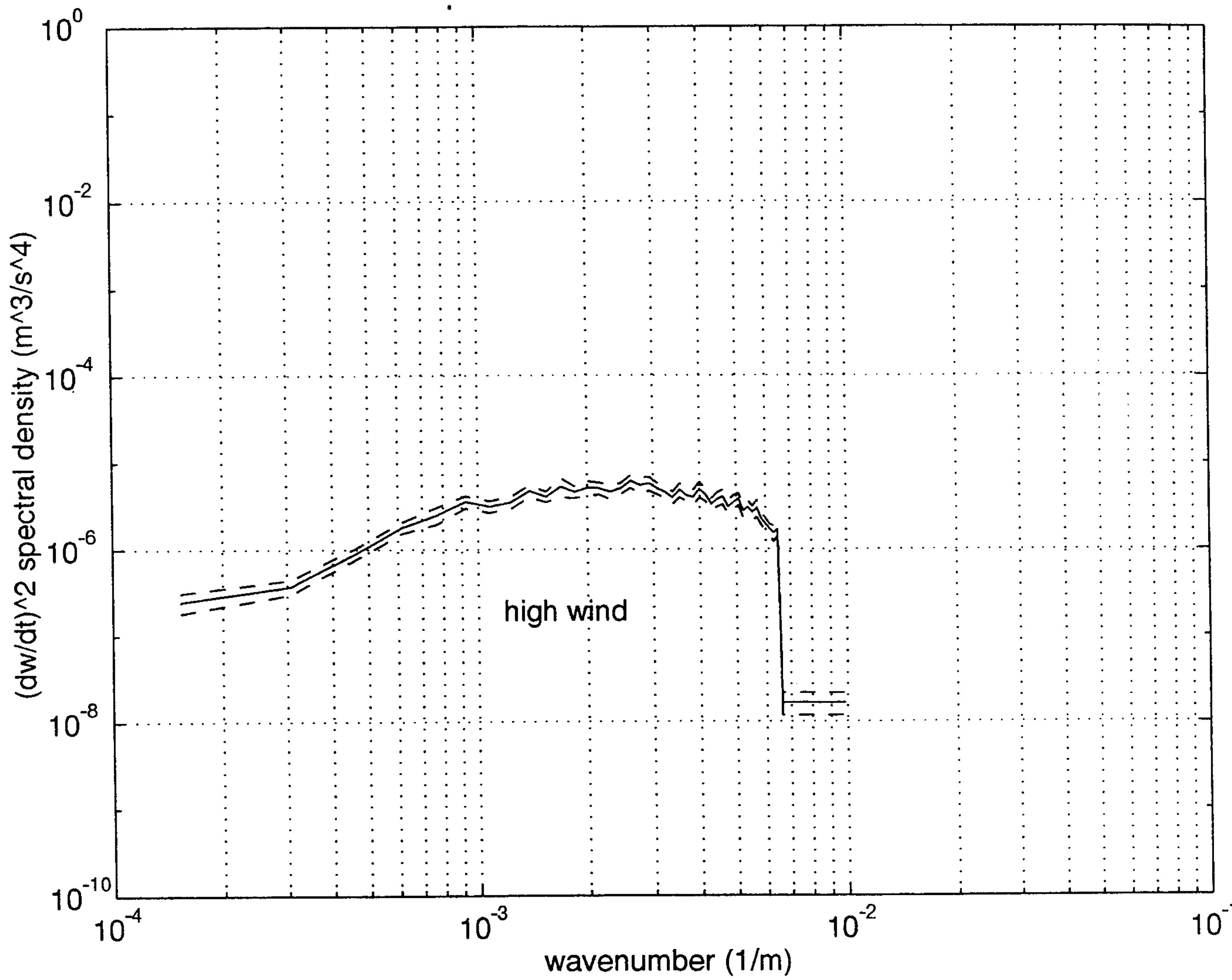

Figure 12. Spectrum of dw/dt from LES Model, Level 3. (dw/dt)^2 spectral density versus wavenumber for the high wind case.

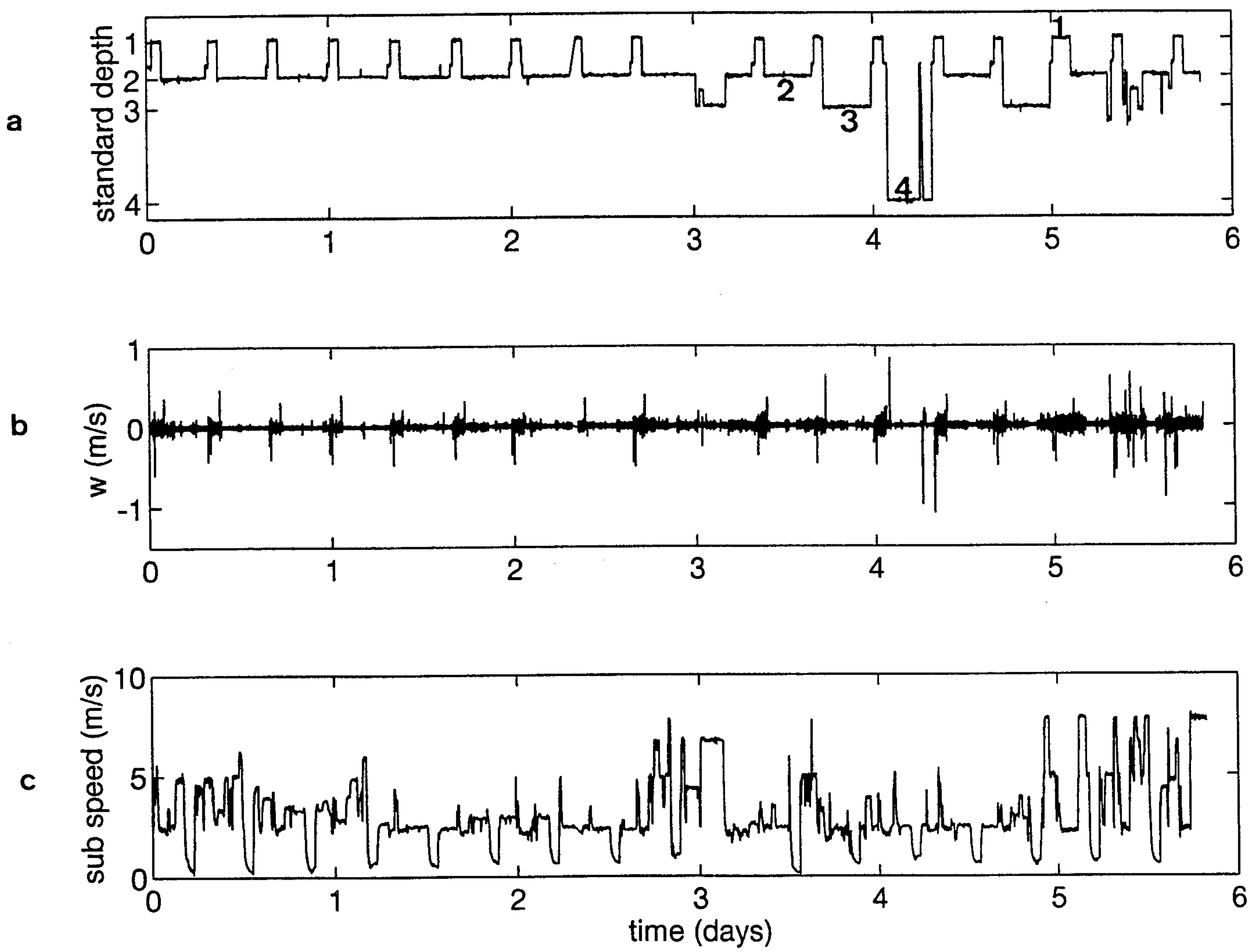

Figure 13. Submarine data record for (a) depth versus time, (b) vertical velocity (w) versus time and (c) submarine speed versus time.

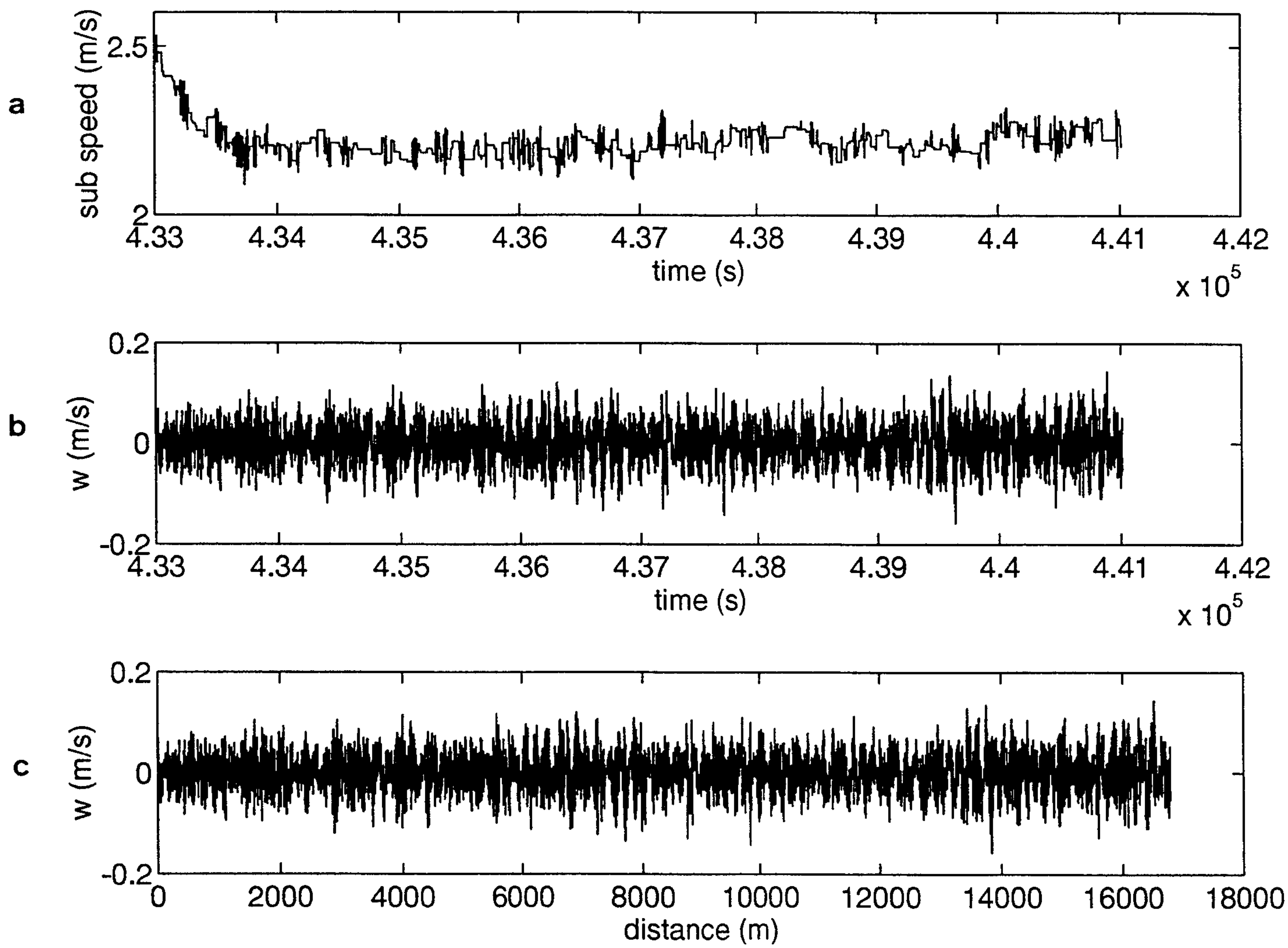

Figure 14. Standard Depth Case 1 for (a) submarine speed versus time, (b) vertical velocity (w) versus time and (c) vertical velocity versus distance.

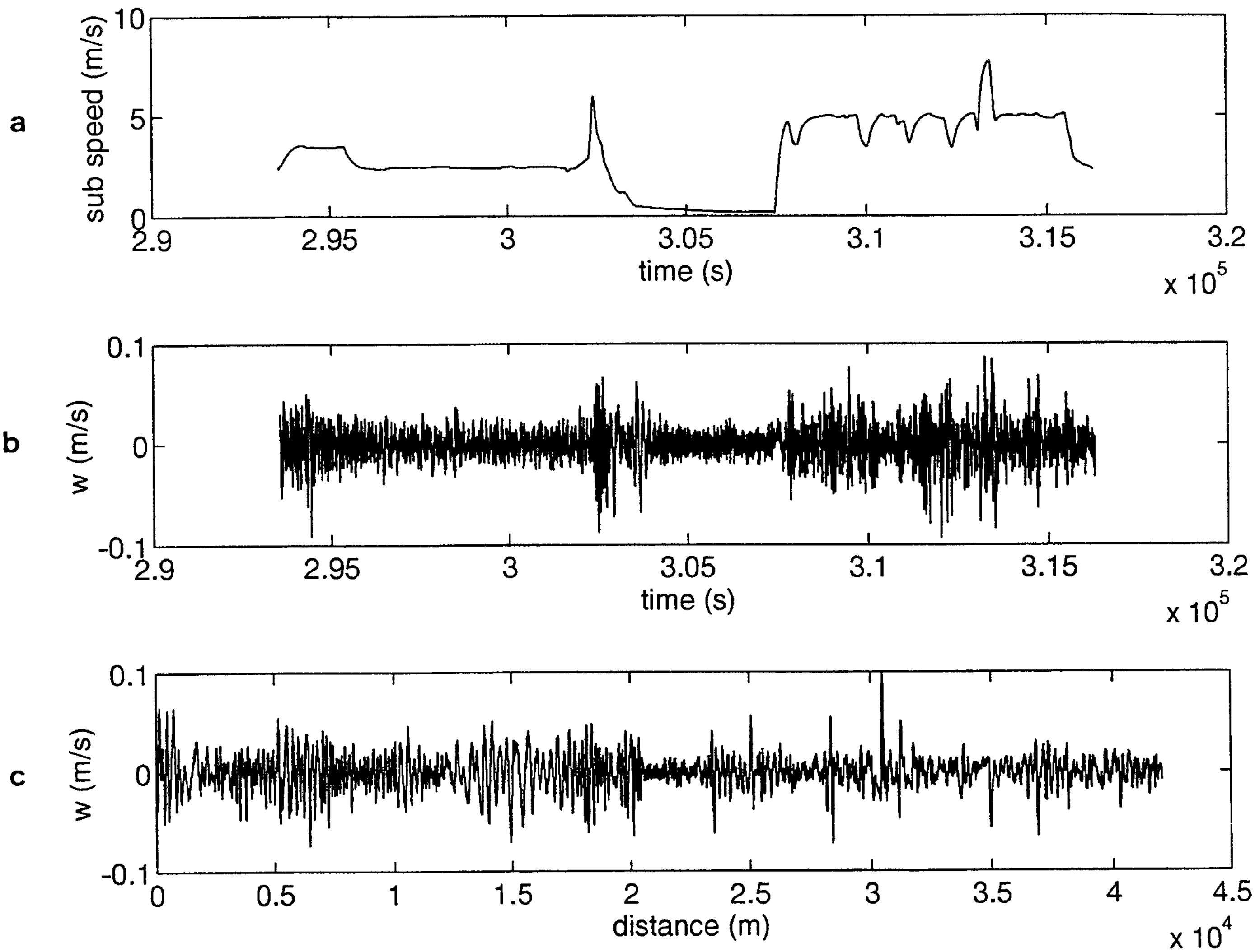

Figure 15. Standard Depth Case 2 for (a) submarine speed versus time, (b) vertical velocity (w) versus time and (c) vertical velocity versus distance.

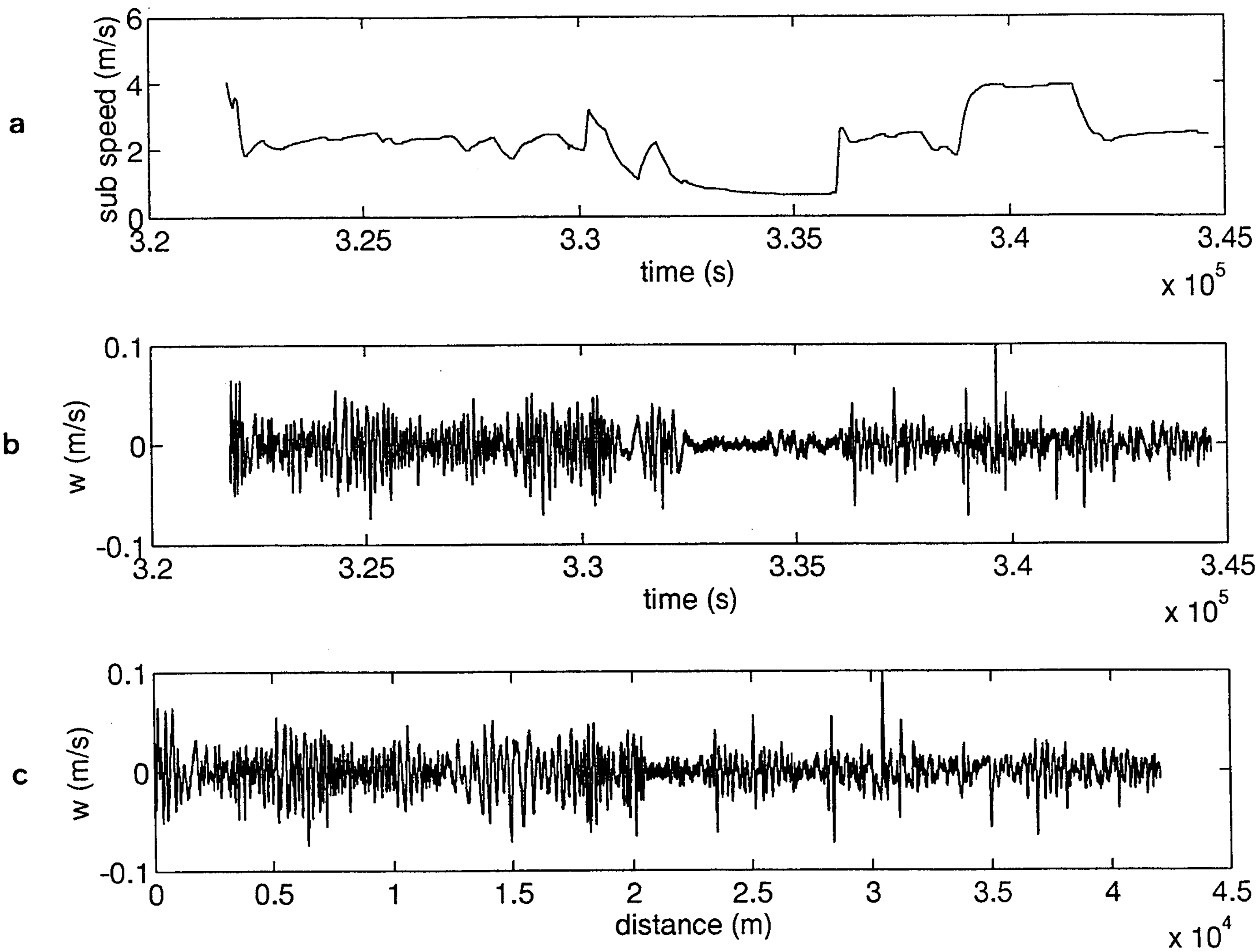

Figure 16. Standard Depth Case 3 for (a) submarine speed versus time, (b) vertical velocity (w) versus time and (c) vertical velocity versus distance.

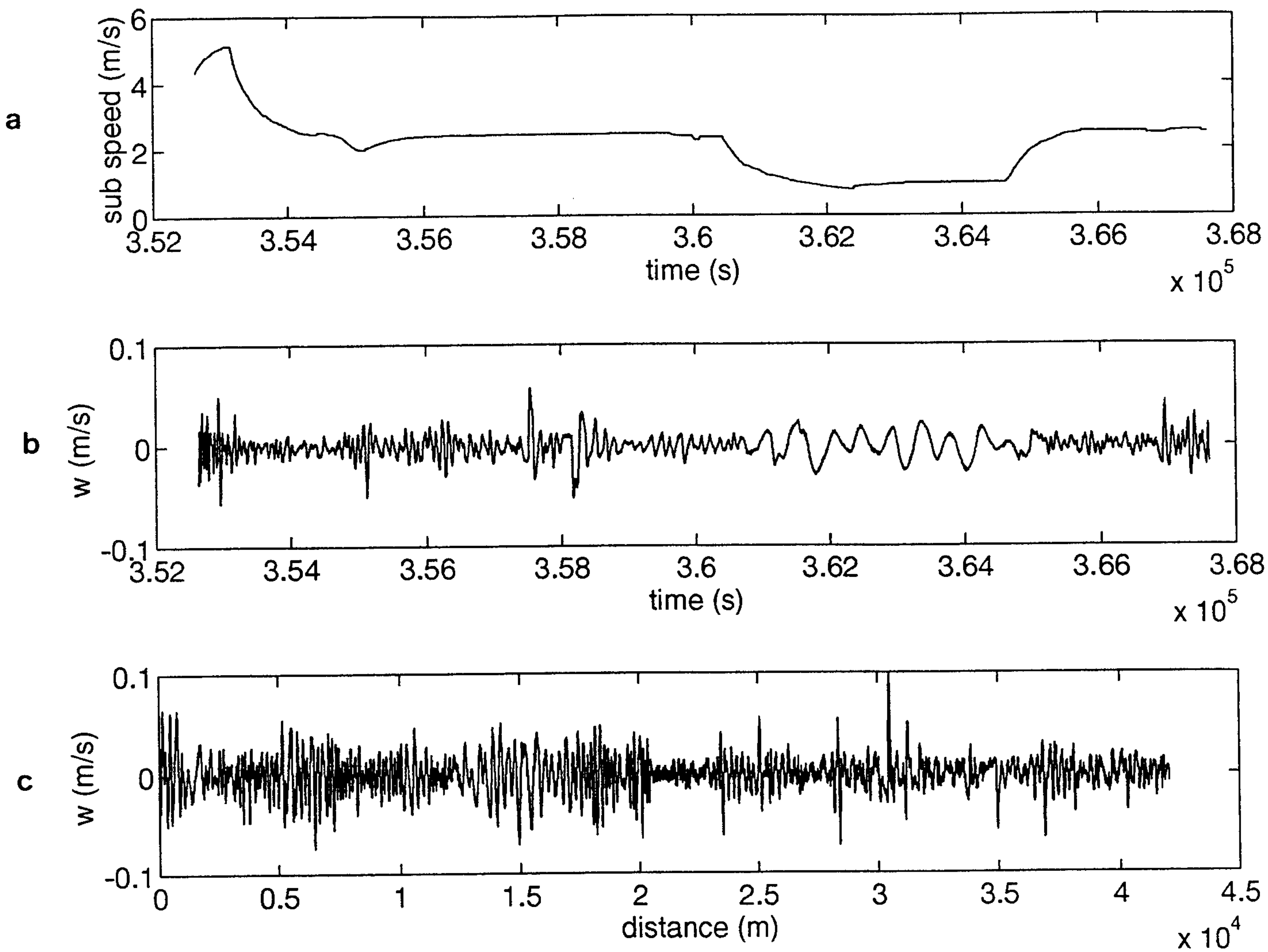

Figure 17. Standard Depth Case 4 for (a) submarine speed versus time, (b) vertical velocity (w) versus time and (c) vertical velocity versus distance.

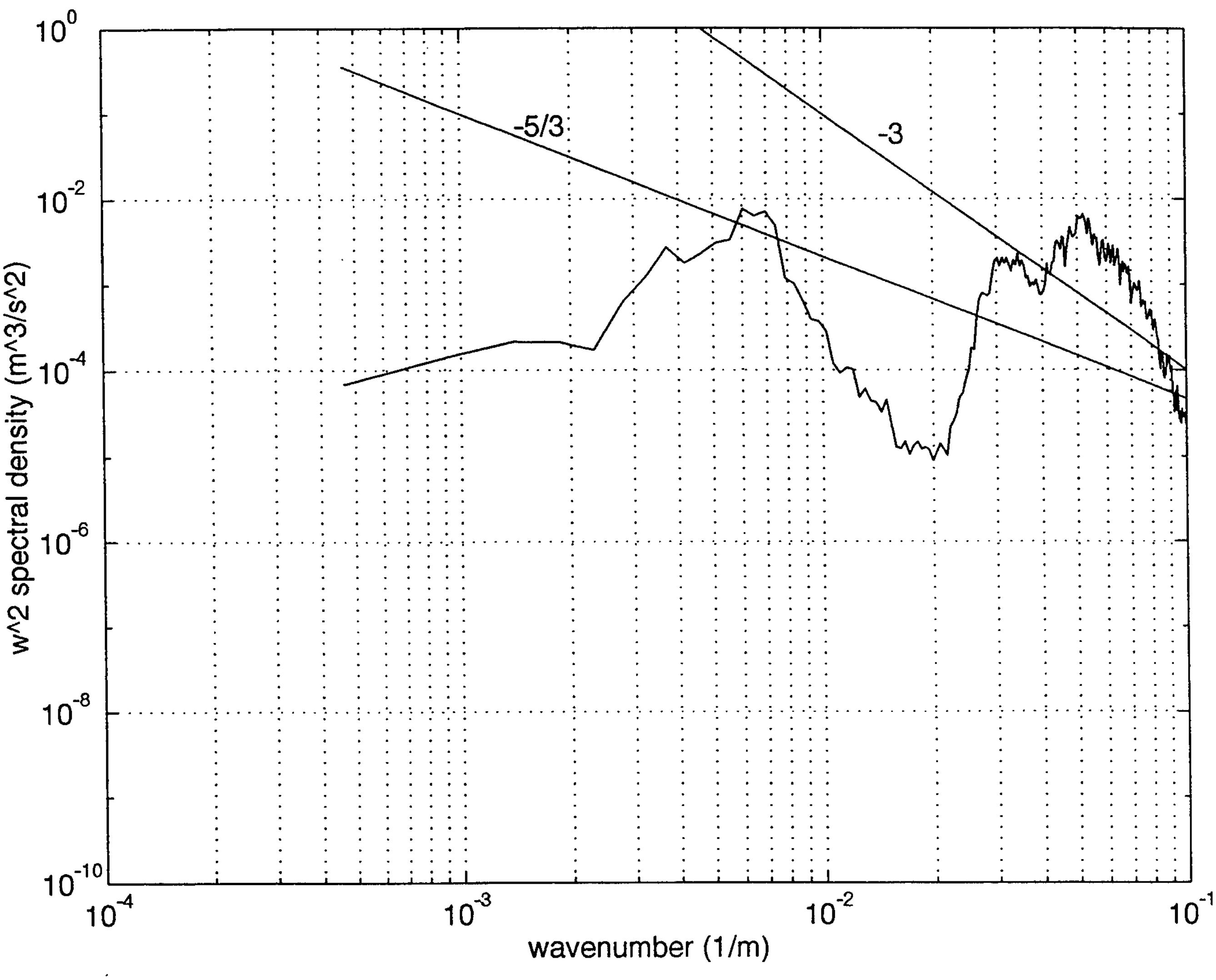

Figure 18. Windowed spectrum of w for Standard Depth 1. w^2 spectral density versus wavenumber.

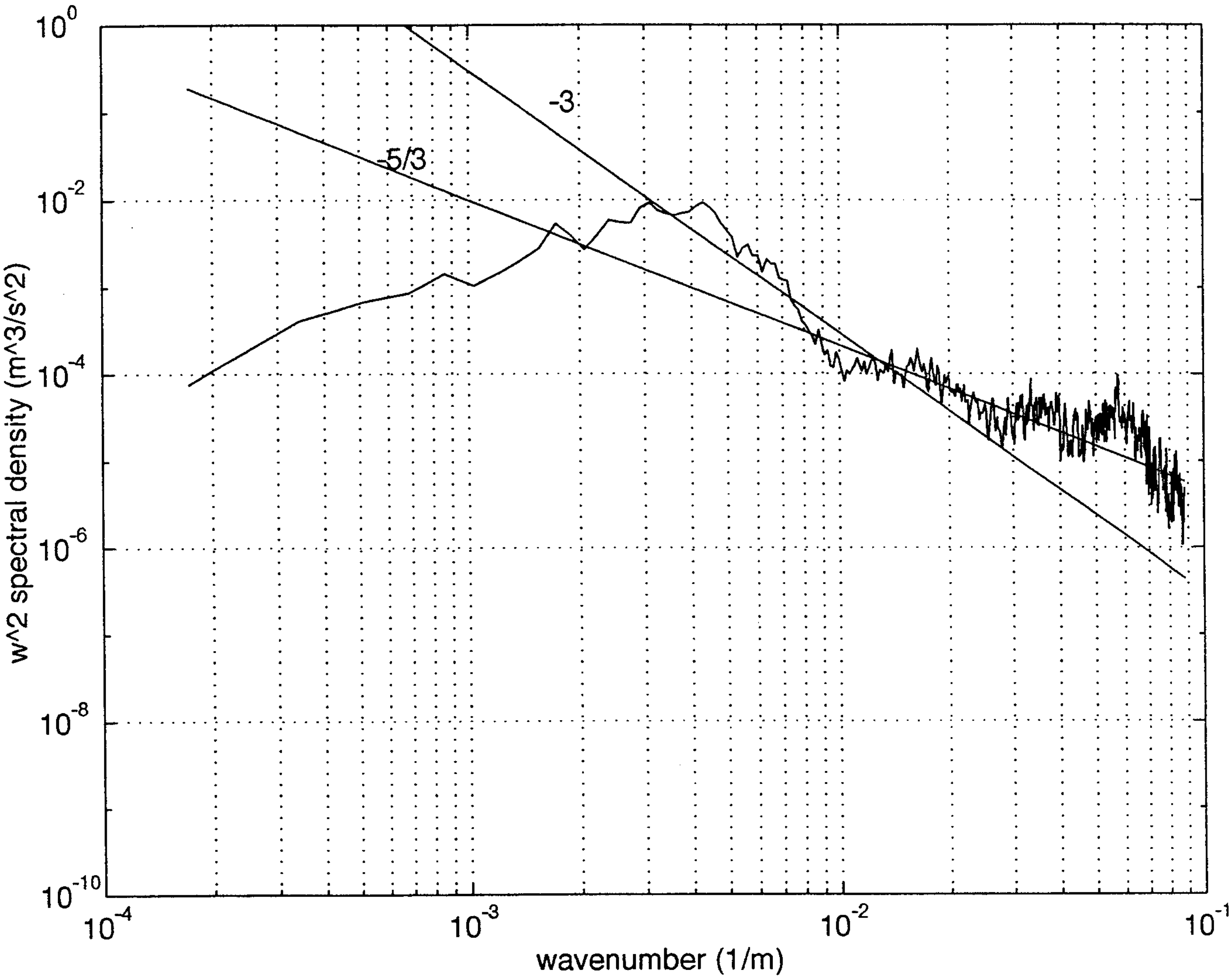

Figure 19. Windowed spectrum of w for Standard Depth 2. w^2 spectral density versus wavenumber.

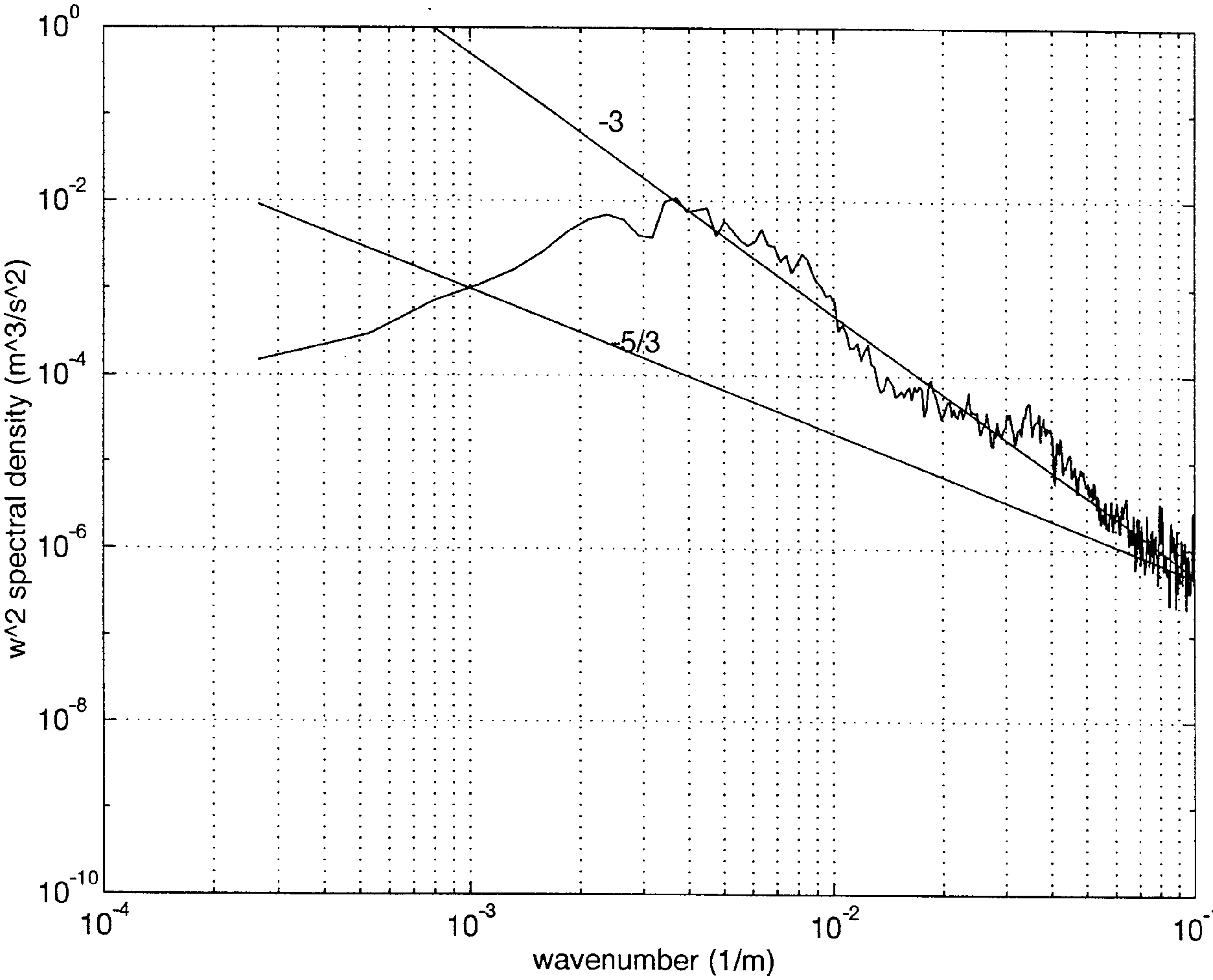

Figure 20. Windowed spectrum of w for Standard Depth 3. w^2 spectral density versus wavenumber.

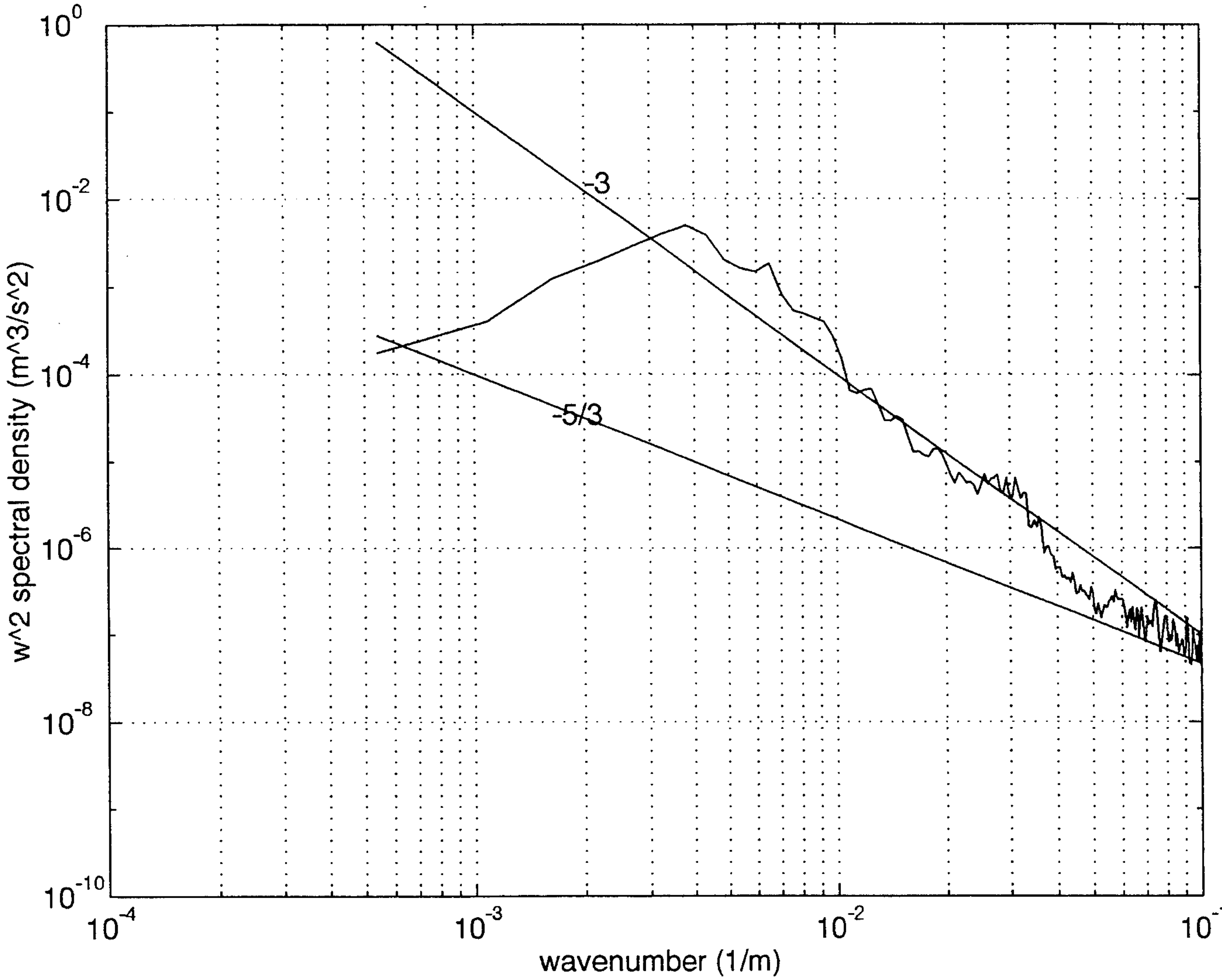

Figure 21. Windowed spectrum of w for Standard Depth 4. w^2 spectral density versus wavenumber.

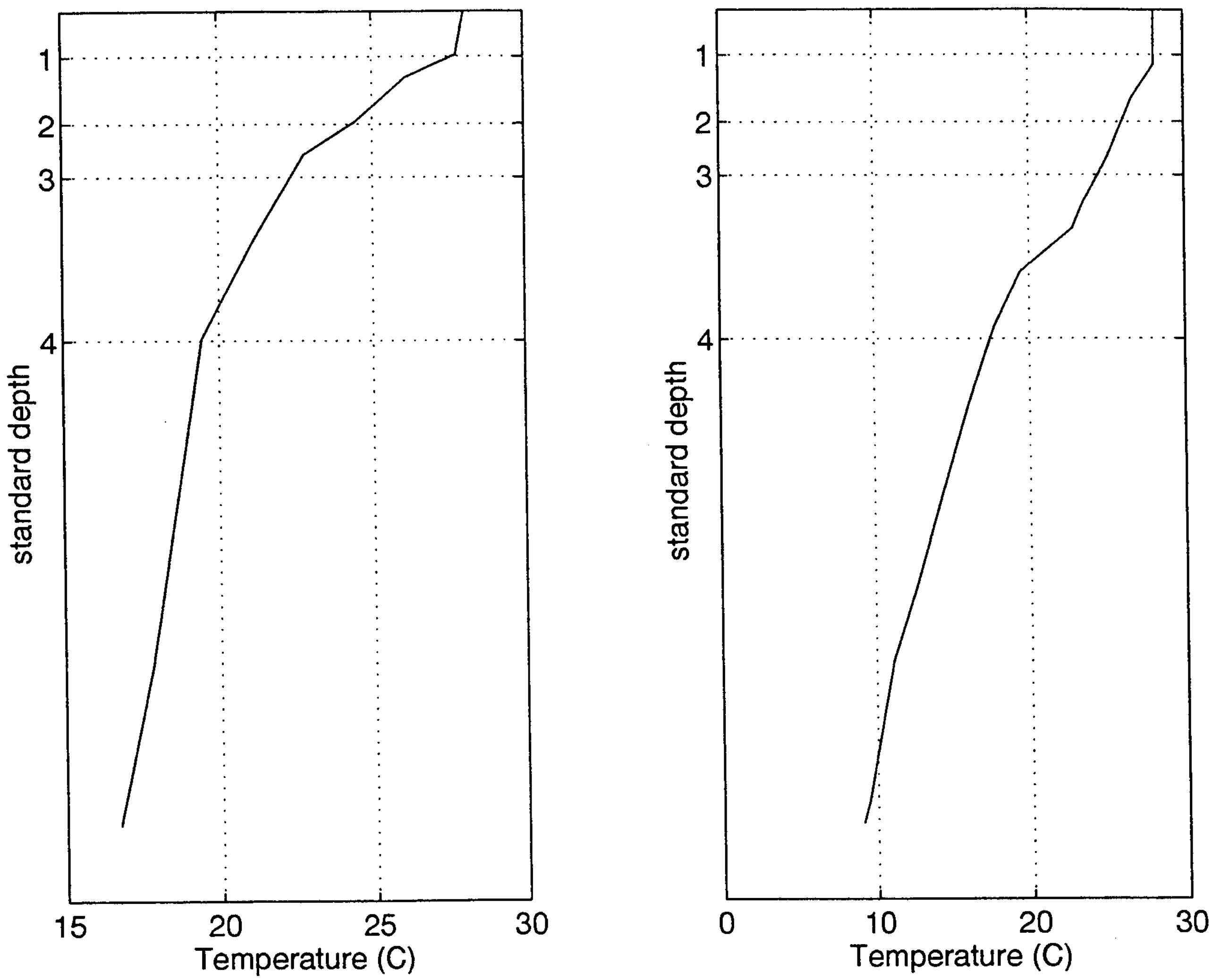

Figure 22. XBT profiles of depth versus temperature, near the location of submarine observations.

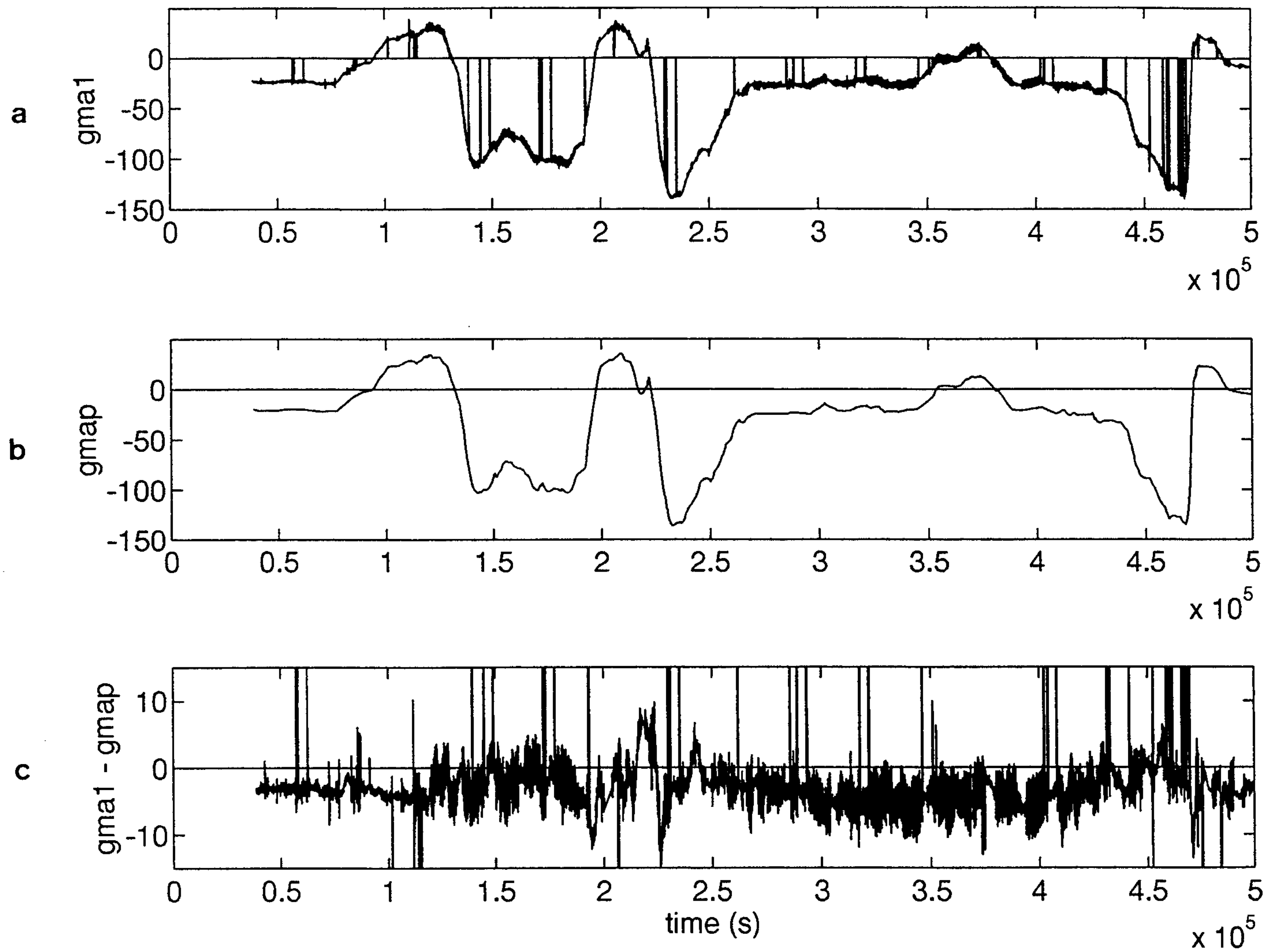

Figure 23. Gravimeter record for (a) observed gravity versus time, (b) gravity anomaly versus time and (c) the difference of (a) and (b) versus time.

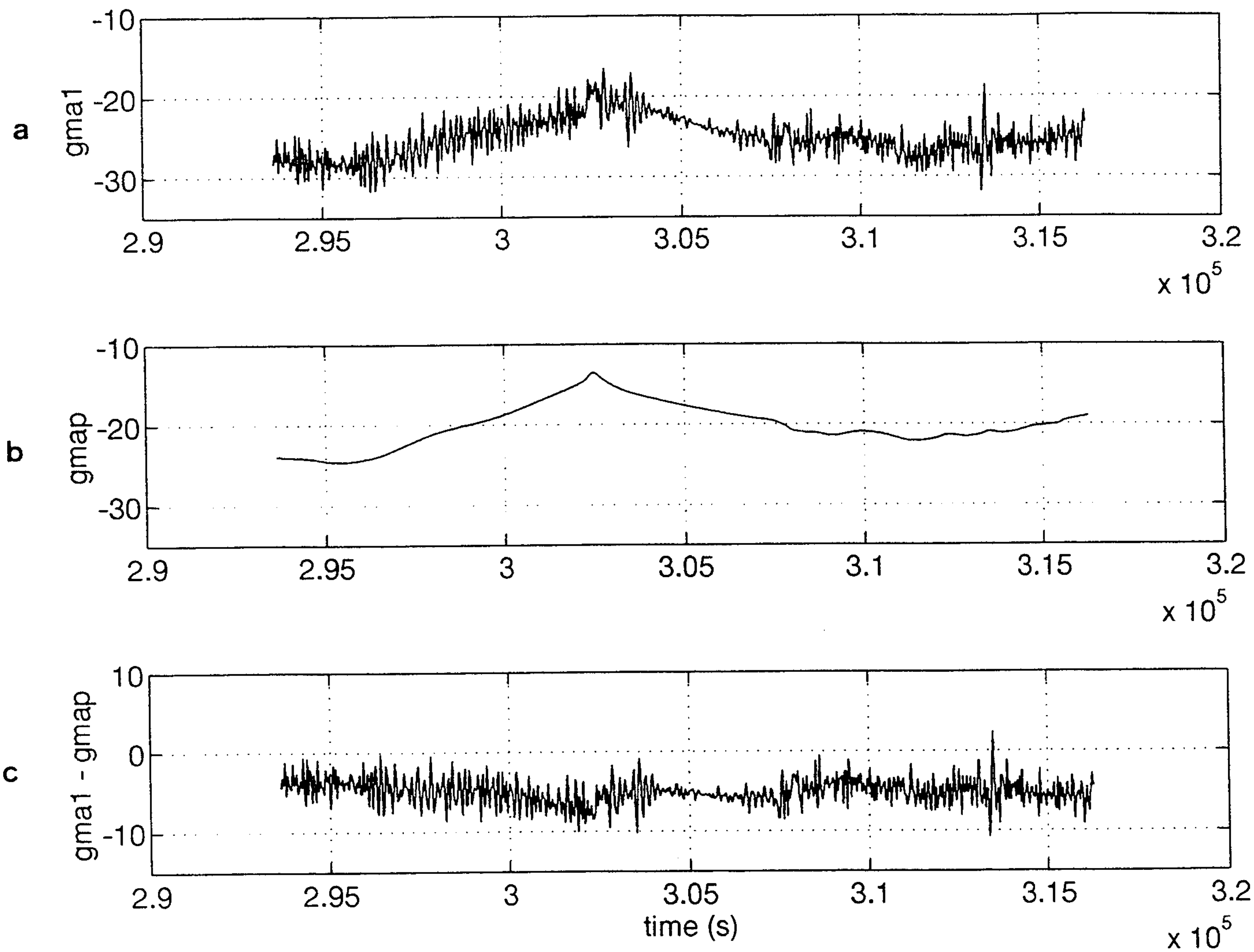

Figure 24. Standard Depth 2. (a) Observed gravity versus time. (b) Gravity anomaly versus time. (c) Observed gravity with gravity anomaly removed.

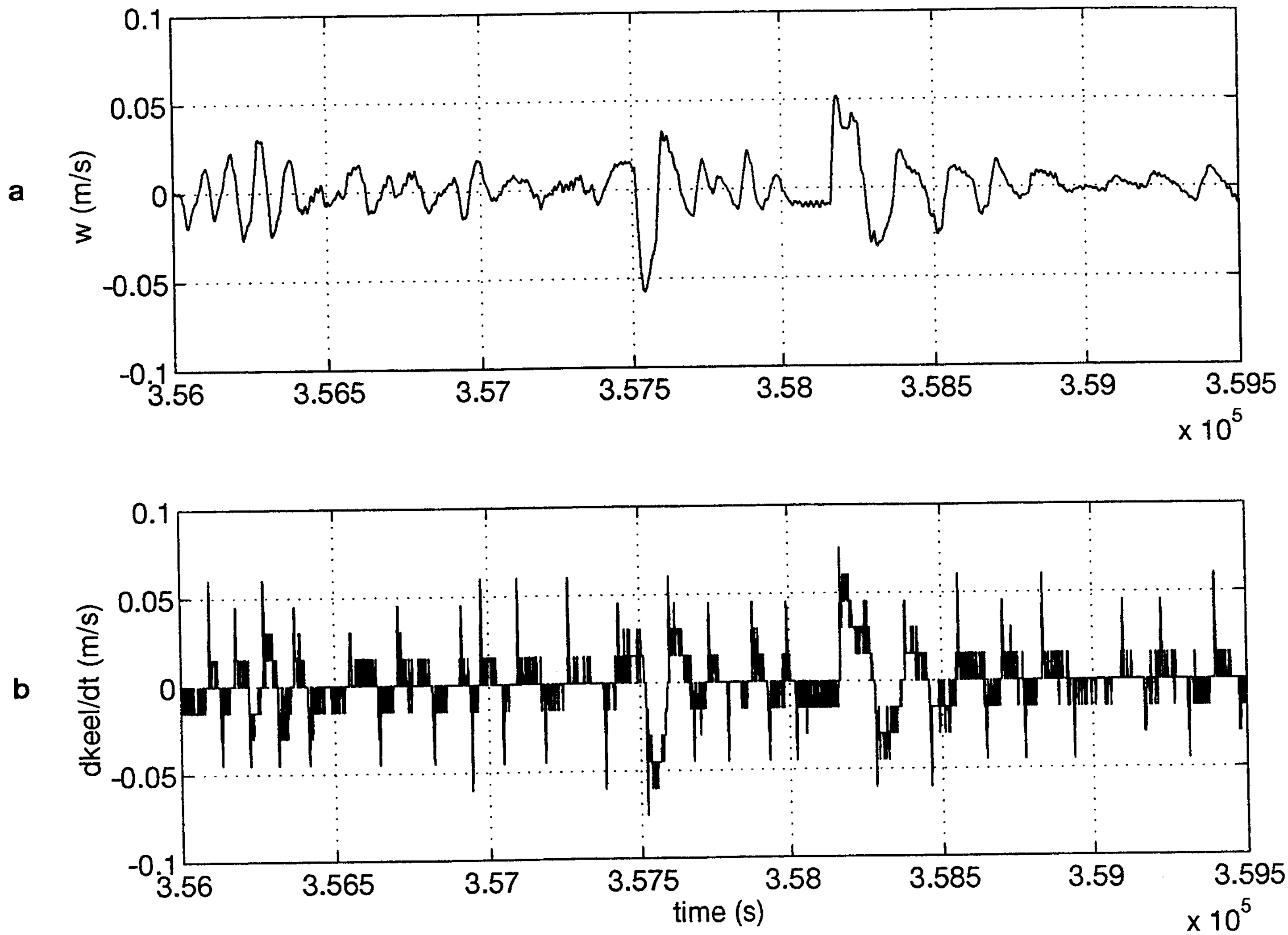

Figure 25. Standard Depth 4 constant speed segment for (a) w versus time and (b) dkeel/dt versus time.

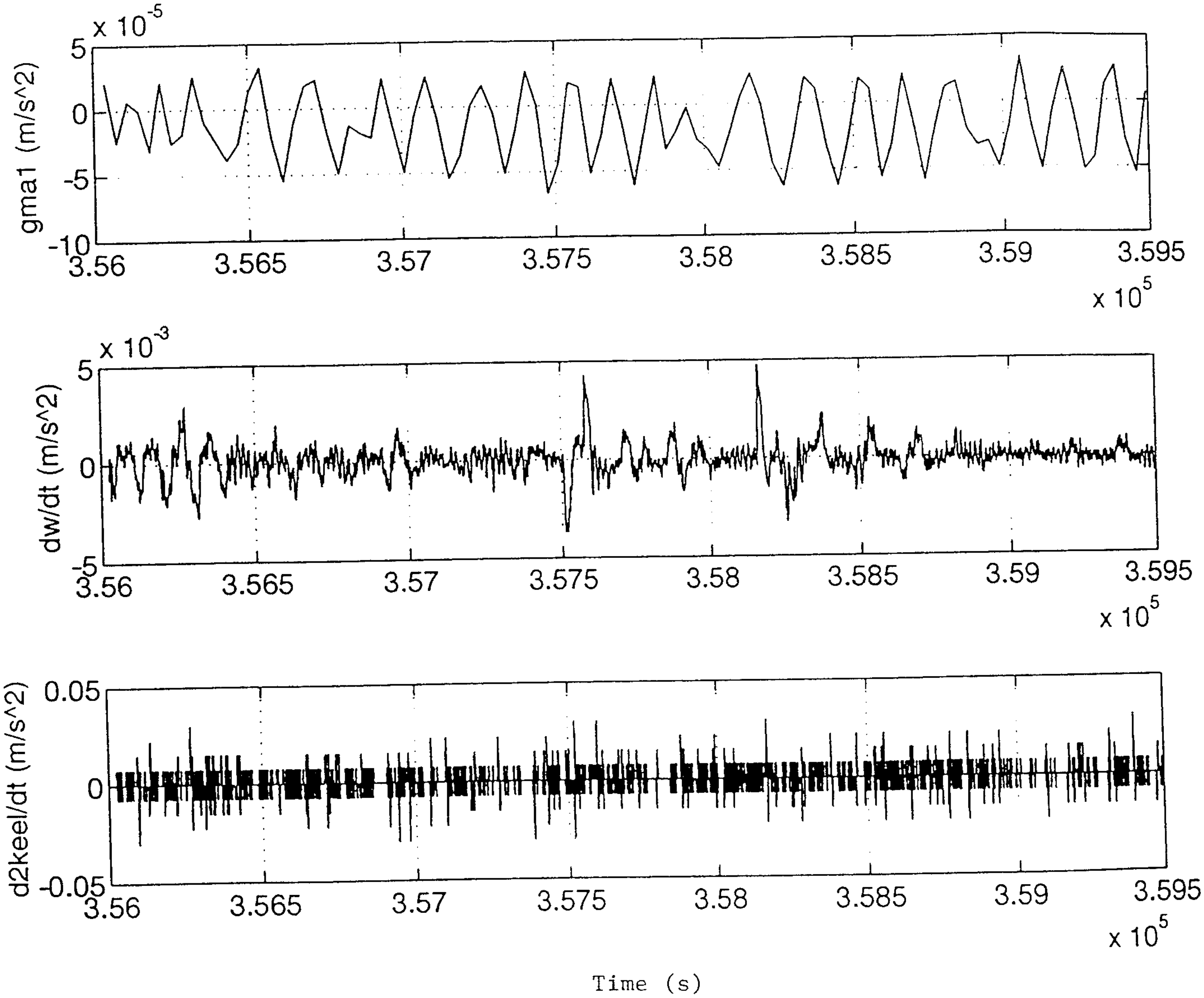

Figure 26. Deep Depth constant speed segment for (a) observed gravity versus time, (b) dw/dt versus time and (c) d^2keel/dt^2 versus time.

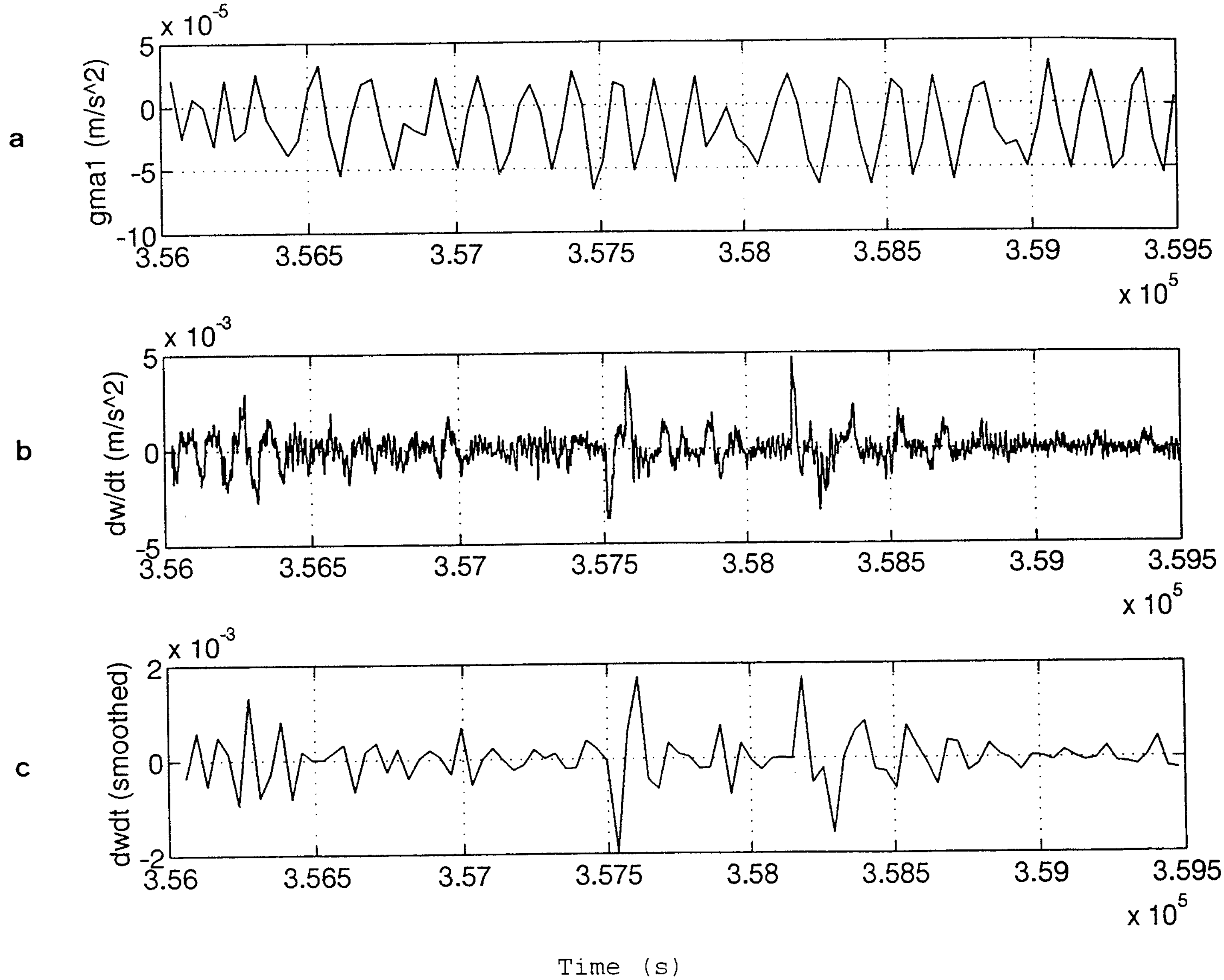

Figure 27. Deep Depth constant speed segment for (a) observed gravity versus time, (b) dw/dt versus time and dw/dt(smoothed) versus time.

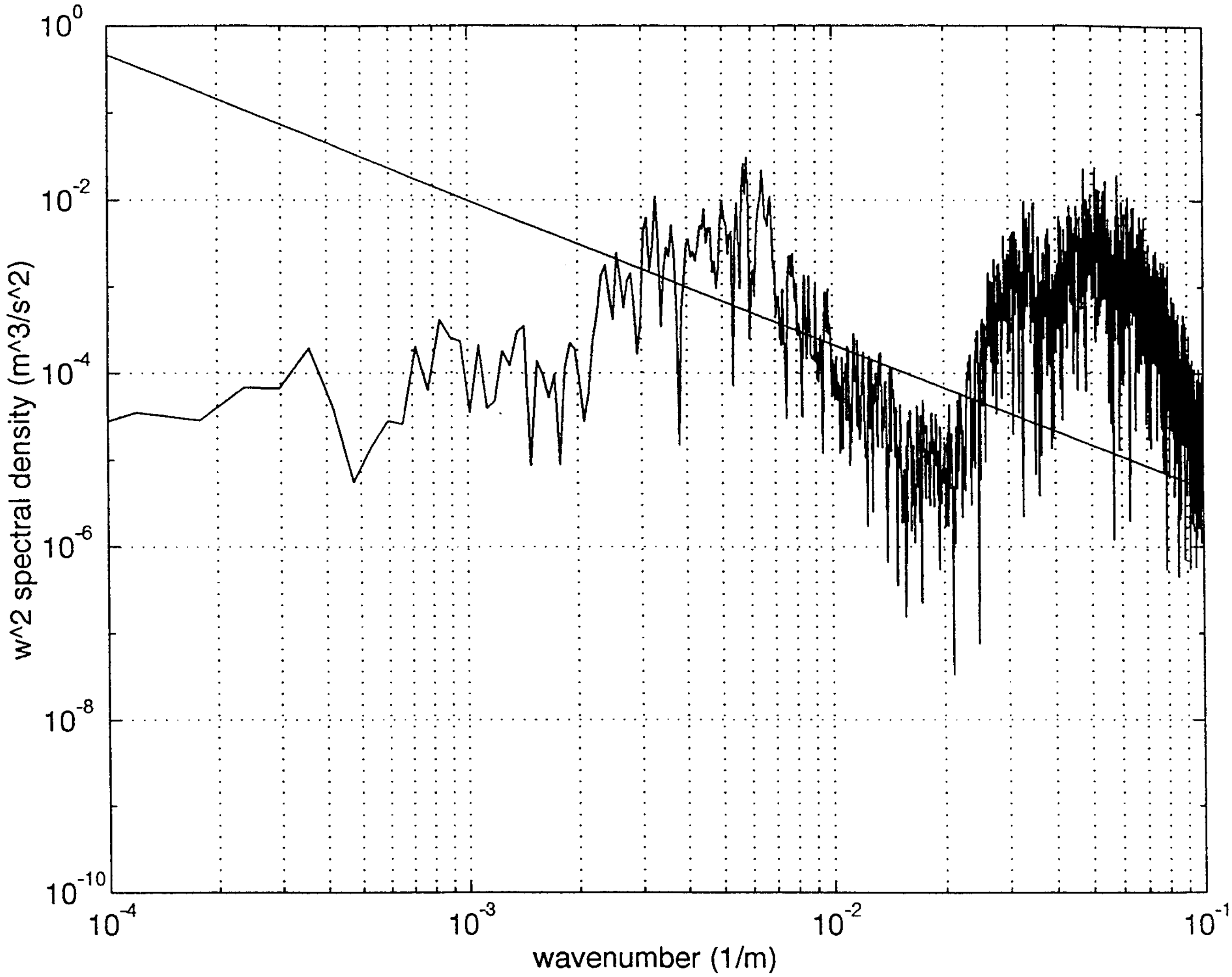

Figure 28. Spectrum of w for Standard Depth 1. w^2 spectral density versus wavenumber.

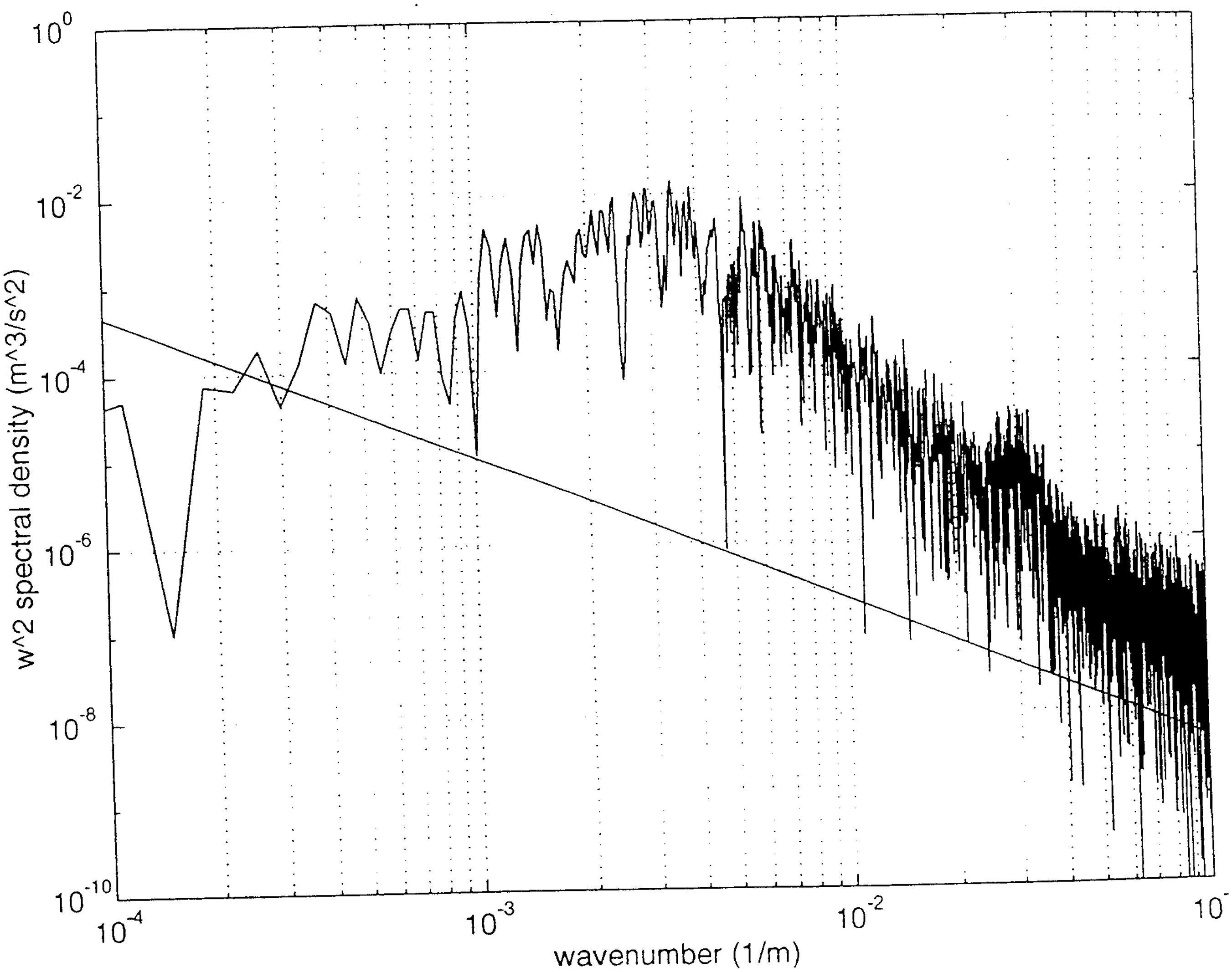

Figure 29. Spectrum of w for Standard Depth 4. w^2 spectral density versus wavenumber.

LIST OF REFERENCES

Aagaard, K., and E.C. Carmack, The Arctic Ocean and Climate: A Perspective, in The Polar Oceans and Their Role in Shaping the Global Environment, eds. O.M. Johannessen, R.D. Muench, and J.E. Overland, Geophysical Monograph 85, American Geophysical Union, 5-19, 1994.

Aagaard, K., L.K. Coachman and E.C. Carmack, On the Halocline of the Arctic Ocean, Deep-Sea Research, 28, 529-545, 1981.

Aagaard, K., J.H. Swift, and E.C. Carmack, Thermohaline Circulation in the Arctic Mediterranean Seas, J. Geophys. Res.,90, 4833-4846, 1985.

Coachman, L.K., and K. Aagaard, Physical Oceanography of Arctic and Subarctic Seas, in Marine Geology and Oceanography of the Arctic seas, ed. Y. Herman, Spring-Verlag, N.Y., 1-81, 1974.

Coachman, L.K. and C.A. Barnes, Surface Water in the Eurasian Basin of the Arctic Ocean, Arctic, 15(4), 251-277, 1962.

Garwood,R.W., Jr., S.M. Isakari, and P.C. Gallacher, Thermobaric Convection, in The Polar Oceans and Their Role in Shaping the Global Environment, eds. O.M. Johannessen, R.D. Muench, and J.E. Overland, Geophysical Monograph 85, American Geophysical Union, 199-209, 1994.

Maykut, G.A., and N. Untersteiner, Some Results from a Time-dependent Thermodynamic Model of Sea Ice, J. Geophys. Res., 76, 1550-1575, 1971.

Mays, M.B. and C.R. Falchetti, Submarine Gravity Measurement Experiment-Phase 1. Naval Air Development Center, Warminster, PA. Report No NADC-78254-40(s), 1978.

McClaren, A.S., The Evolution and Potential of the Arctic Submarine, Oceans '85 Advance Program, San Diego CA, Nov 12-14, 1985.

Moeng, C.-H, A Large-Eddy-Simulation Model for the Study of Planetary Boundary-Layer Turbulence, J. Atmos. Sci., 41, 2052-2062, 1984.

Paluszkiewicz, T., R.W. Garwood, and D.W. Denbo, Deep Convective Plumes in the Ocean, Oceanography, 7, 37-44, 1994.

Pawlowicz R., J.F. Lynch, W.B. Owens, P.F. Worcester, W.M.L. Morawitz and P.J. Sutton, Thermal Evolution of the Greenland Sea Gyre in 1988-1989, J. Geophys. Res., 100, 4727-4750, 1995.

Schilling, C., Submarine Observations of Convection and Mesoscale Phenomena in the Polar Seas (U). M.S. thesis, Naval Postgraduate School, Report No. NPS-OC-93-003, Monterey, 47pp. (Secret document)

Schott,F., M. Visbeck, and J. Fischer, Observations of Vertical Currents and Convection in the Central Greenland Sea During the Winter of 1988-1989, J. Geophys. Res., 98, 14401-14421, 1993.

Scott, J.C., and P.D. Killworth, Upper Ocean Structure in the South-Western Iceland Sea- a preliminary report, in Deep Convection and Deep Water Formation in the Oceans, ed. P.C. Chu and J.C. Gascard, Elsevier Science Publishing Company Inc., Amsterdam , 107-121, 1991.

Stull, R.B., An Introduction to Boundary Layer Meteorology, Kluwer Academic Publishers, Amsterdam, 583pp, 1973.

Turner, J.S., Buoyancy Effects in Fluids, Cambridge University Press, London, 267pp, 1988.

INITIAL DISTRIBUTION LIST

		No. Copies
1.	Defense Technical Information Center Cameron Station Alexandria, Virginia 22304-6145	2
2.	Library, Code 52 Naval Postgraduate School Monterey, Ca 93943-5101	2
3.	Oceanography Department Code OC/Bf Naval Postgraduate School 833 Dyer RD Monterey, Ca 93943-5123	2
4.	Prof. Roland W. Garwood, Jr. Oceanography Department Code OC/Gd Naval Postgraduate School 833 Dyer RD Monterey, Ca 93943-5123	2
5.	Ms. Arlene Guest Oceanography Department Code OC/Gt Naval Postgraduate School 833 Dyer RD Monterey, Ca 93943-5123	2
6.	Dr. Thomas Curtin Office of Naval Research 800 N. Quincy St. Arlington, VA 22217	1
7.	Dr. Manuel Fiadeiro Office of Naval Research 800 N. Quincy St. Arlington, VA 22217	1
8.	Dr. Bernard Epstein Program Management Office Strategic Systems Programs Great Neck, NY 11020-1696	1
9.	Mr. Alan Hayashida NUWC DET Arctic Submarine Laboratory 49250 Fleming Rd. San Diego, CA 92152-7210	1

10. Mr. Jeffrey Gossett 1
NUWC DET Arctic Submarine Laboratory
49250 Fleming Rd.
San Diego, CA 92152-7210

11. Dr. Burton Markham 1
NUWC DET Arctic Submarine Laboratory
49250 Fleming Rd.
San Diego, CA 92152-7210

12. Dr. Diane Bentley 1
NUWC DET Arctic Submarine Laboratory
49250 Fleming Rd.
San Diego, CA 92152-7210

13. Commanding Officer 1
Attn: Mr. Randall Herr
Naval Oceanographic Office
Stennis Space Center, MS 39522-5001

14. LCDR Kevin F. Bedell 1
FLEASWTRACEN, N67
32444 Echo Lane, Suite 100
San Diego, CA 92147-5199